EXPERIMENT AND SIMULATION INVESTIGATION ON AIR BREAKDOWN IN UNIFORM AND NON-UNIFORM FIELD CONFIGURATION

NURUL NATASHA BINTI NGADIMAN

BACHELOR OF ELECTRICAL ENGINEERING
(INDUSTRIAL POWER)
UNIVERSITI TEKNIKAL MALAYSIA MELAKA

"I hereby declare that I have read this report and in my opinion this project is sufficient in terms of scope and quality for the award of the degree of Bachelor of Electrical Engineering (Industrial Power) with Honors"

Signature : ……..

Supervisor's Name : Dr Hidayat bin Zainuddin

Date : 1st JUNE 2017

EXPERIMENT AND SIMULATION INVESTIGATION ON AIR BREAKDOWN IN UNIFORM AND NON-UNIFORM FIELD CONFIGURATION

NURUL NATASHA BINTI NGADIMAN

A thesis submitted in fulfillment

of the requirements for the degree of Bachelor of Electrical Engineering (Industrial Power)

Faculty of Electrical Engineering

UNIVERSITI TEKNIKAL MALAYSIA MELAKA

2017

"I declare that this report entitled "*Experiment and Simulation Investigation on Air Breakdown in Uniform and Non-Uniform Field Configuration"* is the results of my own research except cited in references. The report has not been accepted for any degree and is not currently submitted in candidate of any degree".

Signature : .....

Name : Nurul Natasha bt. Ngadiman

Date : 1st JUNE 2017

Dedicate to my beloved parents and whole of family who always give me support, strength, and encouragement.

ACKNOWLEDGEMENT

First and foremost, I would like to thank Allah whom with His willing gives me the opportunity to complete this Final year Project with successfully before the deadline. Without His permission, I will not be able to reach this stage.

Secondly, I would like to express my appreciation and sincere gratitude to my supervisor, Dr. Hidayat Zainuddin for all this willingness to help me with his conscientious guidance and encouragement that have substantially helped in work. I have greatly benefited from his extensive knowledge and recognized experience in the field of high voltage engineering. It has been a great honour to work with and learn something worthwhile form these amazing people. A big thank you to all the staffs and lecturer in Faculty of Electrical Engineering (FKE), UTeM especially for lecturers from Department of Industrial Power (BEKP) for their useful tips and motivation to finish this study and report on time.

Lastly, I am also greatly thankful to my colleagues for meaningful helps, discussions, and opinions while performing the work in this research. Exceptional gratitude goes to my beloved parents, Hj Ngadiman bin Abd Hamid and Hjh Rosni bin Abdul Manan for their unconditional love and prays while patiently standing beside me along my degree journey. Last but not least, special devotion to my others family members for their endless affection and prays as well as continuous supports and motivations that inspiring my days until the end of the study.

ABSTRACT

This project is concerned with an experiment and simulation investigation on air breakdown in uniform and non-uniform field configuration. An advance improvement in power sector of nation has given a big chance to empower engineers to conserve the power equipment for reliable operation during their operating life. As the high voltage power equipment are mainly subjected with spark over voltage causes by the lightning strokes, a protective device is used to regulate the significant needed for proper insulation level. There are some objectives needed to be achieve in this project. In addition, a series of breakdown strength test was conducted by using AC voltages and the test should be compliance with the required standard, BS EN 60060-1 2010. There are two field configurations used in this study which is plane-plane field configuration with air gap length between 5 until 20 mm and rod-plane field configuration with air gap length between 10 until 50 mm. To determine the AC breakdown voltage, the test voltage is slowly increasing until it reached critical value and breakdown voltage will formed with the validation test of 50 times. 50% disruptive discharge voltage of a test object is used to ensure all measurements are valid according to the standard. U_{50} is prospective voltage value which has a 50 % probability of producing a disruptive discharge on the test object. The value of U_{50} before and after correction, the average, the maximum and minimum value of the field strength along the gap axis, when the breakdown voltage stresses the air gap are recorded and analysed. The results show that the distribution of the field in the gap was affected by the geometry and the arrangement of the gap. For uniform field configurations, as U_{50} was increased, the ability of air to withstand E_{max} (and high stress) was decreased while for non-uniform field configuration, E_{max} was occurred at the tip of the rod which is right on the central longitudinal axis of the rod. It is most likely location where the pre-discharges will occur and followed by air breakdown. The simulation results are compared with relative results of referent work.

ABSTRAK

Projek ini adalah berkaitan dengan siasatan ujikaji dan simulasi voltan jatuhan udara ketika konfigurasi seragam dan tidak seragam. Peningkatan awal dalam sektor tenaga telah memberi peluang besar kepada para jurutera untuk memelihara peralatan kuasa bagi operasi yang boleh dipercayai semasa hayatnya. Peralatan kuasa voltan tinggi tertakluk kepada percikan lebihan voltan disebabkan panahan kilat , maka peranti pelindug digunakan bagi mengawal kesan ketara yang untuk tahap penebat yang betul. Terdapat beberapa objektif yang perlu dicapai dalam projek ini. Di samping itu, satu siri ujian kekuatan telah dijalankan dengan menggunakan voltan AC dan ujian itu haruslah mematuhi standard yang diperlukan iaitu BS EN 60060-1 2010. Terdapat dua konfigurasi medan yang digunakan dalam kajian ini iaitu 'plane to plane' elektrod dengan jurang antara 5 hingga 20 mm dan 'rod to plane' elektrod dengan jurang antara 10 hingga 50 mm. Untuk menentukan AC voltan jatuhan, ujian akan perlahan-lahan meningkat sehingga ia mencapai nilai kritikal dan voltan jatuhan akan terhasil dengan ujian pengesahan daripada 50 kali. 50% pelepasan gangguan voltan objek ujian digunakan untuk memastikan semua ukuran adalah sah mengikut piawaian. U_{50} adalah nilai voltan yang mempunyai kebarangkalian 50% daripada pelepasan gangguan voltan objek ujian. Nilai U_{50} sebelum dan selepas pembetulan, purata, nilai minimum dan maksima kekuatan medan sepanjang paksi direkodkan dan dianalisis. Keputusan menunjukkan bahawa pengagihan bidang dalam jurang terjejas oleh geometri dan susunan jurang. Untuk konfigurasi seragam, apabila U_{50} meningkat, keupayaan E_{max} dalam udara untuk bertahan telah menurun manakala bagi konfigurasi tidak seragam, E_{max} telah berlaku di hujung rod yang tepat pada paksi membujur tengah rod. Ia merupakan lokasi di mana pra-pelepasan akan berlaku dan diikuti oleh voltan udara jatuhan. Keputusan simulasi dibandingkan dengan keputusan relatif kerja rujukan.

Contents

LIST OF TABLES

LIST OF FIGURES

LIST OF ABBREVIATIONS AND SYMBOLS

AC	Alternating Current
ACB	Air Circuit Breaker
AEM	Analytical Element Method
AIS	Air Insulated Substation
BEM	Boundary Element Method
CSM	Charge Simulation Method
FDM	Finite Difference Method
FEM	Finite Element Method
GIS	Gas Insulated Switchgear
HV	High Voltage
OCB	Oil Circuit Breaker
OT	Operating Terminal
SSM	Surface Charge Simulation Method
SF_6	Sulphur Hexafluoride
$U_{50\%}$	50% of breakdown voltage

LIST OF APPENDIX

CHAPTER 1

INTRODUCTION

1.1 Introduction

An advance improvement in power sector of nation has given a big chance to empower engineers to conserve the power equipment for reliable operation during their operating life. It has been seen that the main problem in high voltage power (HV) equipment is the deterioration of the insulation quality of power equipment. As the high voltage power equipment is mainly subjected with spark over voltage causes by the lightning strokes, a protective device is used to regulate the significant needed for proper insulation level [1]. Air at atmospheric pressure is the most necessary gas used for insulating purposes, it has a unique feature of being universally and immediately available at no cost. Furthermore, air has been recommended as environmentally uncritical insulation media for gas insulated electrical power equipment [2], [3]. The resistivity of air can be considered as infinite under normal conditions when there is no ionization [4]. The breakdown of air is very importance to design engineers of power transmission lines and power apparatus [2].

The electric breakdown strength of an air-insulated gap between different metal electrodes can be enhanced considerably by an experiment. In the past decades ago, a lot of research work have been done to improve the understanding about the fundamental characteristics of the electrical breakdown. Therefore, electrical breakdown characteristic of small air gap under the different applied voltage has its great significance for the design of overhead line, substation equipment and various air insulated high voltage equipment [1]. The electrically live conductors are supported on insulating materials and sufficient air clearances

are provided to avoid flashover or short circuits between the live parts of the system and the grounded structures.

The knowledge of electric fields is very basic in numerous high voltage applications. Electric field analysis provides big roles for the development of design and analysis of high voltage equipment, as well as the analysis of various discharge phenomena. The examples of electrode geometries are plane and rod [5]. In order to reproduce the air breakdown voltage has been studied experimentally in high voltage laboratory at Universiti Teknikal Malaysia Melaka (UTeM), brass metal rod of diameter 12 mm and plane of diameter 100 mm are used for measurement of air breakdown voltages and maximum electric field of the high voltage equipment. All the experiments are conducted at the normal temperature and pressure. In addition, the simulation of maximum electric field has been carried out in the COMSOL Multiphysics software. Finally, the experimental results have been compared with theoretical, and simulation results.

1.2 Motivation and Problem Statement

1.2.1 Analytical method

A technique of determining electric field is needed to understand fully behaviour of air under certain electric field profiles. It is difficult to measure properly electric field at all locations between two electrodes. Despite fact the result of experiment test is very accurate and it can validate the simulation results, however in order to conduct each experiment test, a lot of problems will come out especially the equipment needed, cost of maintenance handling and other technical problems. In some electrode geometries, the electric fields can easily be expressed analytically in a closed form solution, but for some cases the electric field problem is complex because of the refined boundary conditions, including media with different permittivity and conductivity [5],[6]. Analytical methods are most choices for simple physical systems as the solving precision and general implementation in most of problems occurred. But, it does not recommended to determine the electric field distributions in the complex arrangements, sometimes in three dimensions [6].

1.2.2 Numerical method

Therefore, to continue this study, it is really recommended to use simulation rather than experiment which is low cost and easy to install. This is because this technique using commercially available electromagnetic software which provides cost effective way and more practical to perform the measurements. Besides, this allows the user to avoid expensive and complex trial-and-error laboratory experiments which are often very difficult to carry out [7]. In order to make comparison between experiment and simulation results, numerical methods are tailored to solve specific problems, usually involving complex geometries where the analytical solution is very complicated or impossible [6]. Although [8] determined the electric field between two spheres by the method of images, numerical simulation techniques, as used by [9], are the preferred method. The comparison between analytical and numerical method as shown in Table 1.1 below.

Table 1.1: The comparison between analytical and numerical method [10].

Analytical Method	Numerical Method
Solve a partial difference equation with initial and boundary conditions.	Replace partial derivative with algebraic equation.
Need solution for each particular problem	One solution can handle multiple problems
Only available for relatively simple problems (homogeneous, simple geometry)	Heterogeneous as well as complex geometry
Example: Analytical Element Method (AEM)	Example: Finite Difference Method (FDM), Finite Element Method (FEM)

The calculation of electrostatic fields requires the solution of Poisson's and Laplace's equations with boundary condition satisfied. There are some numerical techniques that have been used in the literature in for solving Laplace's and Poisson's equations for the fields between complex electrode arrangements. The Poisson equation, widely used in numerical methods, is the main mathematical tool to model the field of the topologies in Fourier series [11]. One of the most successful numerical methods for solving electrostatics field problems is finite element method (FEM). FEM can be employed successfully for the computation of an electric field between electrodes in a medium where one or more dielectrics are involved. The

problem solving of the electric field by FEM is based on the fact, known from variation calculus, while Laplace's equation is achieved when the total energy functional is minimal [5].

1.3 Objectives

The objectives of this report are:

1) To determine the air breakdown voltage and maximum electric field in uniform and non-uniform field configurations.

2) To analyse the experiment results statistically for different electrode configuration.

3) To simulate the electric field for different electrodes configurations by using COMSOL Multiphysics software.

4) To compare the results between an experimental testing and simulation method.

1.4 Scope of Works

The scopes of this study are:

1) Tests on air breakdown voltage is carried out to investigate U_{50} and the results are corrected according to the correction factors defined by the standard in BS EN 60060-1 2010 (high-voltage test techniques) to ensure the accuracy of the results are reliable.

2) Gap length between electrode configurations start with 5 mm, 10 mm, 20 mm, 30 mm, 40 mm and 50 mm are used to measure the air breakdown voltage and maximum electric field of high voltage equipment.

3) The simulation of maximum electric field using uniform and non-uniform field configurations (plane-plane and rod-plane electrode configurations) is simulated by using COMSOL Multiphysics software.

CHAPTER 2

LITERATURE REVIEWS

2.1 Introduction

This chapter contains a literature review that related to this research. All information and related theory such as the power system applications, air breakdown mechanism, classical gas laws, estimation and control of electric stress and numerical methods for computation of electric field are studied and discussed in this chapter. Furthermore, the review of previous related works regarding to this research are also discussed. Although many experimental works and tests have been carried out and presented by researchers, there are still gaps that needed to be filled in order to convince the working committee to make comparison of maximum electric field using different electrodes configuration.

2.2 Power System Applications

2.2.1 Circuit breaker application

Air circuit breaker (ACB) has brilliant function as to provide short circuit and overcurrent protection for circuits ranging from 800A to 10,000A. There are two types of air circuit breaker which is air circuit breaker and air blast circuit breaker. ACB has completely replaced by oil circuit breaker (OCB). The use of air circuit breaker is usually used in low voltage applications below 450V while air blast circuit breaker is high capacity breakers and can be used substations above 132kV. Furthermore, the operation between these two circuit breakers are quite different and in different countries, ACB still a preferable choice as there is no chance of oil fire like in OCB [12]. The operation and construction of ACB are easy, simple and inexpensive. Fire hazards will not occur in case of insulation damage of the cabinet as in

the case of OCB. The other applications of ACB such as protection of plants, electrical machines and also used for protection of transformers, capacitors and generators [12].

2.2.2 Air- Insulated Substation (AIS) application

AIS uses air as the main dielectric from phase to phase, and phase to ground insulation. AIS also had been used for a long time before the introduction of gas insulated substation (GIS). Furthermore, AIS is more comprehensive use in areas where space, weather conditions and environmental concerns are not a big issue such as rural areas, and favourable terrain [13]. AIS is also an essential choice for areas with a large space, low cost of system constructions and low maintenance as all the equipment is within view. However, due to modern technology and economic nowadays, GIS offers the best choice rather than AIS. For the engineers and technician, the choice between GIS and AIS depends on the pros and cons between these two [13].

2.3 Air Breakdown Mechanism

2.3.1 Collision Processes

There are two types of collisions which are elastic collisions and inelastic collisions. Elastics collisions are collisions when only kinetic energy gets readjusted while there is no change takes place in the internal energy of the particles. When electrons strike with gas molecules, a single electron traces a zig-zag path during its journey. Since electrons are very light in weight, they send only a part of kinetic energy to the much heavier ion or gas molecules with which they collide. Inelastic collisions are those in which internal changes in energy take place within an atom or a molecule at the expense of the total kinetic energy of colliding particle. The structure of the atom depends on the collision results [2].

2.3.2 Townsend's Mechanism

Townsend's mechanism is based upon:

- Ionization collision in the gas
- Ionization collision on the surface of the electrodes
- Photo-ionization

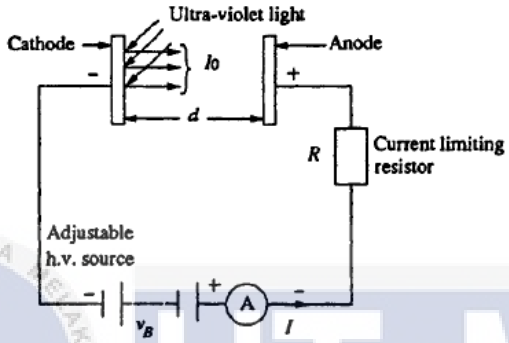

Figure 2.1: Arrangement for study of a Townsend discharge [2].

Figure 2.1 shows the arrangement for Townsend's discharge. Ionization is the way towards an electron from a gas particle with the synchronous generation of a positive particle. In the process of ionization by collision, a free electron collides with a neutral gas particle and offers to another electron and positive ion. Based on Figure 2.8, when there is low pressure column in which an electric field E is applied across two plane parallel electrodes on that point, any electron starting at the cathode will be accelerated among collisions with different gas molecules during its travel towards the anode [2]. Ionization will be happen if the energy (ε) obtained during this travel between collisions higher than the ionization potential, V_i as the process can be represented as below

$$\varepsilon > V_i$$
$$e^- + \mathrm{A} \longrightarrow e^- + A^+ + e^- \qquad (2.1)$$

where, A is the atom, A^+ is the positive ion and e^- is the electron.

The additional electron, then, themselves make 'ionizing collisions' and thus the process repeats itself. This represents an increase in the electron current, since the number of electrons is reaching the anode per unit time is greater than those liberated at the cathode. In addition, the

positive ions also reach the cathode and on bombardment on the cathode give rise to secondary electrons. Figure 2.2 shows the current-voltage relationship based on Townsend theory and have four stages during the process to breakdown [2].

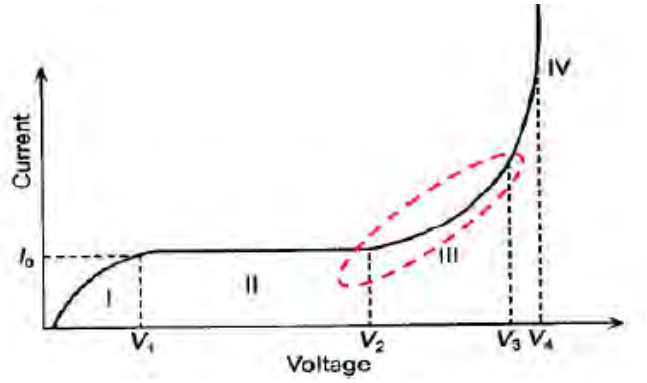

Figure 2.2: The current-voltage relationship based on Townsend Theory [2].

Townsend's mechanism process has several stages to breakdown occur. When the region I, at the low voltage, current increased linearly (not steady) with the voltage up to saturation level (I_O) when all electron available are conducting.

When the region II, the current is almost constant while region III, after V_2, the current rises exponentially. The exponential current to ionization of the gas by electron collision. As the field rises, electrons leaving the cathode are accelerated vigorously between collisions until they get enough energy to cause ionization on collision with gas molecules or atoms [14]. As the gap voltage, V increases in the gap, the electric field, E (E=V/d usually defined in kV/cm or V/cm) increases. Thus, the probability of the ionization increases due to the collision of electron with uncharged particle. The rapid increases of ionization processes in the gap region are called avalanches process.

When the region IV, anode current will be increased sharply. The current magnitude could reach infinity and the value is limited only by the external resistance. Even the current behaviour would not change even if the UV light source is removed and the process is independent. Finally, the gas is to be breakdown [2].

Drawbacks of Townsend Theory

Townsend mechanism explains the breakdown phenomena only at low pressure, corresponding to gas pressure x gap distance (p x d) values of 1000torr-cm and below (1 atm = 760 torr). In

addition, current growth is due to ionization processes in parallel plate gap only without considering other factors as practical and actual conditions were shown as Table 2.1 below

Table 2.1: The comparison between practical and actual condition of Townsend Theory [2].

Practice	Actual
Breakdown voltage depend on gas pressure and geometry.	Breakdown observed to occur at very short time of the order of 10^{-8}s.
Townsend predicts breakdown time(time lags) of the order of 10^{-5}s	Townsend predicts a much diffused form of discharge where it was found to be filamentary and irregular.
In 1940, Raether, Meek and Loeb introduced the Streamer Theory	

2.3.3 Streamer Theory of Breakdown in Air

The Townsend Mechanism failed to explain the observed phenomena and streamer theory is proposed. The growth of charge carrier in avalanche in a uniform field $E_0 = V_0/d$ is described by the $e^{\alpha d}$. This statement is valid only as long as the electrical field of the space charges of electrons and ions can be neglected compared to the external field E_0 [14]. Raether [15][16] reported that when charge concentration was between 10^6 to 10^8, the growth of an avalanche became weak *i.e.,* $dn/dx < e^{\alpha d}$ based on the effect of space charge on avalanche growth. The avalanche current will increase when the charge concentration bigger than 10^8 and breakdown of the gap occurred. During high concentration, fast growth will occurred as slow growth take place during low concentration [2],[15],[16]. Figure 2.3 shows the streamer mechanism which have several process, there were :

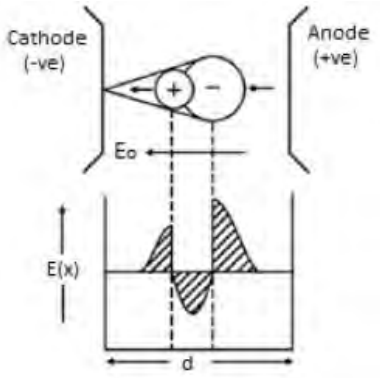

Figure 2.3: Streamer mechanism of breakdown in air [2].

a) Process 1

Ionization process by collision causes negative charges to anode and positive charge to cathode. This process will create avalanches of electron that must have lighter and higher mobility compare to positive ion. Therefore the electron will be filled the head and positive ion occupied the tail.

b) Process 2

Space charges by ionization will distort the uniform field. The spherical volumes concentrate at negative charges at the head and positive charge at the tail. The field behind and a head of avalanches is increase by the space charge, ε_r. The field between the electron and the cloud is reduced. Alpha *d* increased, field distortion increases. Alpha is an average number ionization made by one electron per unit drift in the direction of the field. When alpha, *d* at critical value, space charges field is comparable to ε_0. This condition created an intense ionization and excitation of the gas particle in front of the avalanches head. Excited atoms return to normal immediately. The process will release of photon, which turns generate secondary electron by the photo ionization process. The generated secondary electrons from the photo-ionization will generate further auxiliary avalanches as a Figure 2.8. Since photons travel with the speed of light, the process leads to rapid development of conduction channel across the gap and develop as self-propagating streamer. The streamer proceeds across the gap and to form a conducting filament of high ionized gas between electrodes, the gas was breakdown [2],[15],[16].

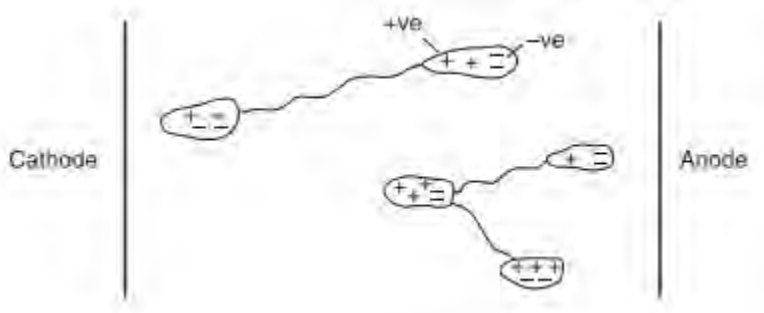

Figure 2.4: Development of secondary avalanches due to photo-ionization [15].

2.3.4 Paschen's Law

As referred to the Townsend's criterion for breakdown equation which is

$$1 - \gamma[\exp(\propto d) - 1] = 0 \quad (2.2)$$

where the coefficients $\propto$ and γ are functions of E/p, i.e

$$\frac{\alpha}{p} = f_1\left(\frac{E}{p}\right)$$

and

$$\gamma = f_2\left(\frac{E}{p}\right)$$

also

$$\mathrm{E} = \frac{V}{d}$$

Substituting for E in the expression for $\propto$ and γ and rewriting, the final equation will be f_2

$$\left(\frac{V}{pd}\right)[\exp\{pdf_1\left(\frac{V}{pd}\right)\} - 1] \quad (2.3)$$

This equation shows a relationship between *V* and *pd*, and implies that the breakdown voltage varies as the product *pd* varies. Knowing the nature of the functions f_1 and f_2, it can rewrite as

$$V = f(pd) \quad (2.4)$$

This equation is known as Paschen's law and has been experimentally established for various gases, and it is very important law in high voltage engineering [2]. The relationship between *V* and *pd* is shown in Figure 2.5 which is the Paschen's curve for three gases of CO_2, air and H_2. It is obvious that the relationship between *V* and *pd* is not linear and has a minimum value for any gas. Based on Table 2.3 , there are the lists of minimum breakdown voltages for various gases.

Table 2.3 : The lists of minimum breakdown voltages for various gases [2].

Gas	V_s min (V)	*pd* at V_s min (torr-cm)
Air	327	0.567
Hydrogen (H_2)	273	1.15
Carbon Dioxide (CO_2)	420	0.51
Nitrogen (N_2)	251	0.67
Oxygen (O_2)	450	0.7

When the values of $pd > (pd)_{min}$, electrons crossing the gap make more frequent collisions with gas molecules than at $(pd)_{min}$, but low energy gained between collisions. There are more voltage has to be applied to maintain the desired ionization while for the values of $pd < (pd)_{min}$, electron may cross the gap without even making a collision or making only less number of collisions. Therefore, more voltages are needed for breakdown to occur [2]. The breakdown potentials for uniform field gaps in air, CO_2 and H_2 at 20°C are shown in Figure 2.5

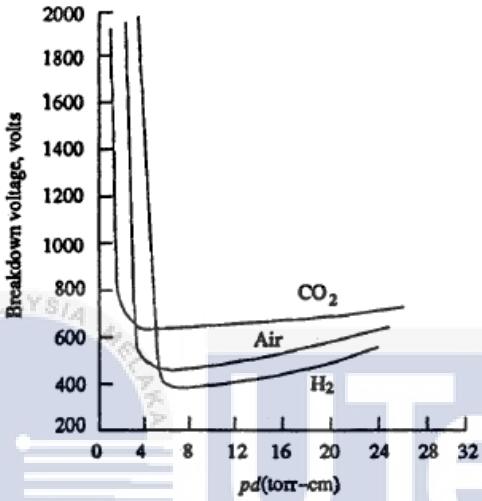

Figure 2.5: The breakdown potentials for uniform field gaps in air, CO_2 and H_2 at 20°C [2].

In order to cater the effect of temperature, the Paschen's law is generally stated as $V = f(Nd)$ where N is the density of the gas molecules. This is fundamental because the pressure of the gas changes with temperature according to the gas law pv = NRT, where v is the volume of the gas, R is constant and T is the temperature. The breakdown potential of air can be expressed as

$$\mathrm{V} = 24.22\,[\frac{293pd}{760T}] + 6.08\left[\frac{293pd}{760T}\right]^{1/2}\left[\frac{293pd}{760T}\right]^{1/2} \tag{2.5}$$

as the breakdown voltage at constant pressure and temperature is not constant.

At 760 torr and 293°K,

$$\mathrm{E} = V/d = 24.22 + [\frac{6.08}{\sqrt{d}}]\ \mathrm{kV/cm} \tag{2.6}$$

while this equation yields a limiting value for E of 24kV/cm for long gaps and a value of 30kV/cm for $([\frac{293pd}{760T}]) = 1$, which means a pressure of 760 torr at 20°C with 1 cm gap. This is usually breakdown strength of air at room temperature and at atmospheric pressure.

2.4 Classical Gas Laws

In the absence of electric or magnetic fields charged particles in weakly ionized gases participate in molecular collisions. Their movements take after nearly the classical kinetic gas theory. Boyle and Mariotte state that in oldest gas law experiment, the product of pressure (p) and volume (V) is constant for a given amount of enclosed gas at a constant temperature [14] or

$$pV = \mathrm{C} = \mathrm{const} \tag{2.7}$$

When the pressure is remain constant during the same system, the volumes V and V_0 are related to their absolute temperature T and T_0 (in K) by Gay-Lussac's law:

$$\frac{\mathrm{V}}{V_0} = \frac{T}{T_0} \tag{2.8}$$

If the temperatures are expressed in degree Celsius, equation (2.8) becomes

$$\frac{V}{V_0} = \frac{273 + \theta}{273} \tag{2.9}$$

Based on equation (2.9) suggests that as nearly θ = - 273 ℃ the volume of gas decreases to zero but in actual, all gases liquefy before reach this value. According to eqn (2.8) the constant C in eqn (2.7) is related to a given temperature T_0 for the volume V_0:

$$\mathrm{p}V_0 = C_0 \tag{2.10}$$

By substituting V_0 from eqn (2.8) gives

$$\mathrm{p}V = (\frac{C_0}{T_0})\mathrm{T} \tag{2.11}$$

Universal gas constant is the ratio ($\frac{C_0}{T_0}$) and it represent by R. Then equation (2.11) will becomes

$$\mathrm{p}V = RT = C \tag{2.12}$$

which is R is a constant independent of the nature of the gas and it is equal to 8.314joules/°K mol. If take n as the number of moles, i.e the mass m of the gas divided by its mol-mass, based on equation (2.13) and it will becomes an ideal gas

$$pV = nC = nRT \tag{2.13}$$

Eqn (2.13) also can be written in terms of gas density N in volume V containing N_1 molecules which is $N = N_A$ where N_A is known as the Avogadro's number and it is equal to 6.02 x 10^{23} molecules/mole, eqn (2.7) becomes

$$\frac{N_1}{V} = N = \frac{N_A}{R}\frac{p}{T}$$

or

$$pV = \frac{N_1}{N_A} RT = N_1 kT \tag{2.14}$$

or

$$p = NkT$$

When constant $k = \frac{R}{N_A}$ is the universal Boltzmann's constant (=1.3804 x 10^{-23}joules/°K) and N is the number of molecules in the gas. During the same temperature and pressure, when two gases with initial volumes V_1 and V_2 are combined, the new volume will be given by

$V = V_1 + V_2$ or in general $V = V_1 + V_2 + V_3 + \ldots + V_n$ (2.15)

After combining eqn (2.13) and (2.15) gives

$$V = \frac{n_1 RT}{p} + \frac{n_2 RT}{p} + \cdots + \frac{n_n RT}{p}$$

After rearrange,

$$p = \frac{n_1 RT}{V} + \frac{n_1 RT}{V} + \cdots + \frac{n_1 RT}{V} \tag{2.16}$$

$$\text{or } p = p_1 + p_2 + \ldots + p_n$$

where p_1, p_2, … , p_n denote the partial pressures of gases 1, 2, …, n and equation (2.16) is generally referred to as the law of partial pressures. Moreover, eqn (2.7) until (2.16) can be derived directly from the kinetic theory of gases developed by Maxwell in the middle of the nineteenth century [14] .

2.5 Estimation and Control of Electric Stress

2.5.1 Electric Field

When the concepts of electric fields is presented, it is very necessary for high voltage engineers to learn of field intensities in various media under electric stresses. It also helps in determining proper electrode configurations and economical dimensioning of the insulation [2]. The field intensity **E** at any location in an electrostatic field is the ratio of the force on an infinitely small charge at that location to the charge itself as the charge decreases to zero. The force **F** on any charge q at that point in the field is given by [17]

$$\mathbf{F} = q\,\mathbf{E} \tag{2.17}$$

The electric flux density **D** associated with the field intensity E is

$$\mathbf{D} = \varepsilon\,\mathbf{E} \tag{2.18}$$

In electrostatics, Maxwells's equations and constitutive equation reduce to following form

$$\nabla \times E = 0 \tag{2.19}$$

$$\nabla . D = \rho \tag{2.20}$$

$$\mathbf{D} = \varepsilon\,\mathbf{E} \tag{2.21}$$

where **E** is the electric field intensity, **D** is the electric displacement, ρ is the space charge density, ε is the dielectric permittivity of the material. Based on equation (2.19), electric field is introduced by the negative gradient of the electric scalar potential V in the following form

$$E = -\nabla V \tag{2.22}$$

Substituting equations (2.20) and (2.21) in (2.19) Poisson's scalar equation is obtained as

$$-\nabla.(\varepsilon\nabla V) = -\nabla.(\varepsilon_0\varepsilon_r\nabla V) = \rho \quad (2.23)$$

Where ε_0 is the permittivity of the free space, $\varepsilon_r = \varepsilon_r$(E, x, y, z) is the relative permittivity and ρ is the space charge density. If the permittivity ε is constant such as in the isotropic dielectrics, equation (2.23) becomes

$$\Delta V = -\rho\varepsilon \quad (2.24)$$

For space charge free ($\rho = 0$) fields, field is expressed by Laplace's equation as $\Delta V = 0$

2.5.2 Uniform and Non-Uniform Electric Field

In common, the electric fields between any two electrodes can be either uniform or non-uniform field. The average field **E** is constant throughout the field region in a uniform field gap [18]. Uniformity in an electric field can be approximated by placing two conducting plates parallel to one another and creating a potential difference between them or two spheres of equal diameters when the gap distance is less than diameter of the sphere as shown in Figure 2.6 below [2],[19]. Sometimes, parallel plates of finite size are used to produce uniform electric fields, when plate size is much bigger than gap separation [2]. According to [2],[20],[21] the uniform electric field between two parallel electrodes separated by a distance d is proportional to the voltage :

$$E_{mean} = \frac{V_{mean}}{d} \quad (2.25)$$

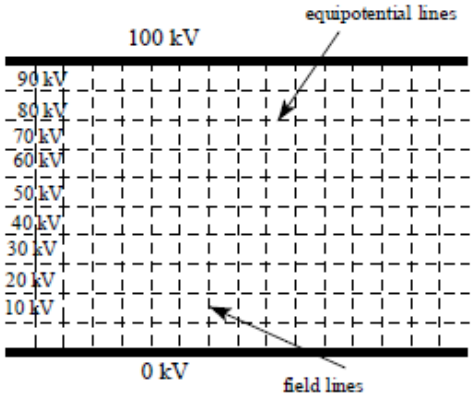

Figure 2.6: Uniform electric field between two parallel plates [19].

Unlike in a non-uniform field gap, **E** is different at different points of the field region. The insulation breakdown in non-uniform fields take place after stable partial discharge (pre discharge) are set. The pre discharges are rendered unstable just before the breakdown [18]. If the electrodes are curved, the field strength is not constant throughout the region. An example of a non-uniform electric field is shown in Figure 2.7. The straight line represents the critical field line, which corresponds to the point with the shortest distance to the grounded plane. The maximum electric field always occurred at the tip of the needle. Because of its sharpness, this point shows an extremely big field "concentration" and at the same time a steep fall around it [22].

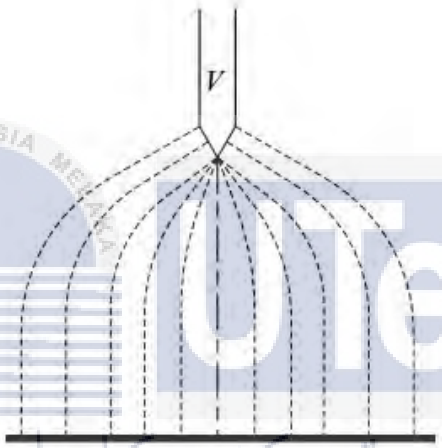

Figure 2.7: Non-uniform electric field [22].

2.5.3 Degree of Uniformity of Electric Fields

The degree of uniformity η (eta) was introduced by Schwaiger in 1922 as a measure of the uniformity of a field, is defined as following

$$\eta = \frac{E_{mean}}{E_{max}} \tag{2.26}$$

where E_{mean} and E_{max} are the peak values of the mean and the maximum field intensities respectively [18] as E_{mean} can be obtained in eqn (2.25). The value of η also represents the degree of utilization of the dielectric in between any two electrodes. Besides, it compares the ideal condition of electric field intensity (uniform field between electrodes at the same distance *d* apart) with the existing actual maximum field intensity. Thus η, a dimensionless quantity

enables to make comparison of the uniformity of fields formed between different electrode configurations. Table 2.4 gives the values of η in electric fields. The values of η lies between

$$0 \leq \eta \leq 1 \tag{2.27}$$

Table 2.4: The values of η in electric fields [18].

Field classification	Uniform	Weakly non-uniform	Extremely non-uniform
Electrode Configuration	Parallel plates	Concentric sphere	Needle-plane
η	1	0.25	≪0.01

2.6 Numerical Methods for Computation of Electric Field

In these few years, there are some numerical methods to solve partial differential equations which consists of Laplace's and Poisson's equation have become available. There are basic difficulties in solving these equations for two or three dimensional fields with complex boundary conditions, or for insulating materials with different permittivity and conductivity [2].

A good design of any high voltage equipment needs a full knowledge of the electric field distribution. However, there are some cases where the physical systems are very complicated and therefore in such cases, numerical methods are selected for the calculation of electric fields. As common in high voltage engineering applications, there are four types of numerical methods which are divided into two different methods which are domain and boundary methods. Finite Element Method (FEM) and Finite Difference Method (FDM) are represent domain methods while Charge Simulation Method (CSM) and Surface Charge Simulation Method (SSM) or Boundary Element Method (BEM are represent boundary methods. The principal methods used are shown in Figure 2.8 [2],[19]. Furthermore, the relative advantages and disadvantages of the various numerical methods are shown in Table 2.5 below. For this study, there is only one method focused which is FEM.

Table 2.5: The relative advantages and disadvantages of the various numerical methods [2].

	Advantages	Disadvantages
Finite Element Method (FEM)	1. Very general method and can be solve a variety of problems. 2. Any linearity or inhomogeneity can be modelled. 3. The solution available on the entire surface of the domain.	1. A powerful graphic user interface for processing.
Finite Difference Method (FDM)	1. Simple but time consume. 2. Subdivide the finite plane of the field problem into a predominantly regular net.	1. Large resulting error.
Charge Simulation Method (CSM)	1. Very smooth, easy to handle 2. The solution satisfies the Laplace's/Poisson's equation.	1. Non-linearities and non-homogeneity cannot be modelled.
Boundary Element Method (BEM)	1. Electric fields are proportional to the charge densities on an enclosed electrode which is simulated by real changes. 2. Field derivation based on Gauss's area integral.	1. Program complex and need large amount of computational time to execute an improper integral.

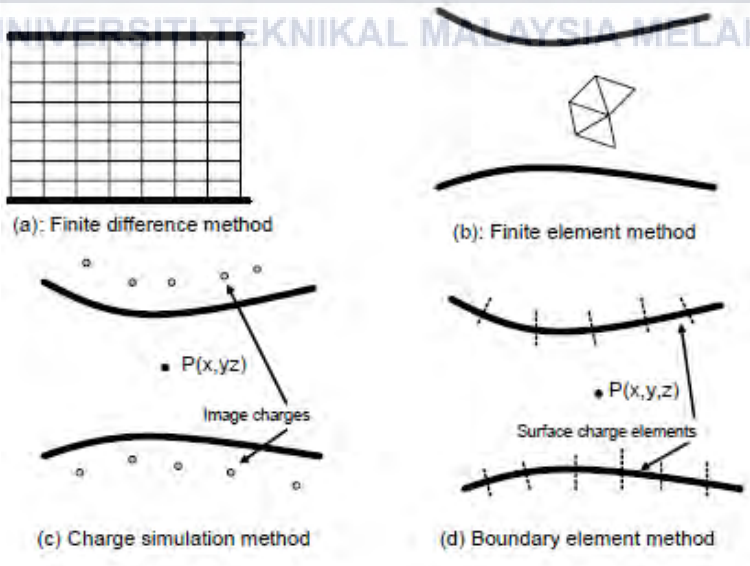

Figure 2.8: Principal methods of field simulation [19].

2.6.1 Finite Element Method (FEM)

Finite Element Method is favored and extensively used in the numerical solution of electric field problems. By comparing with other numerical methods, FEM is a very adaptable tool and common method in order to solve a lot range of electric field problems [2]. It is also a convenient way for fields with many dielectrics, inhomogeneous and non-linear materials, for complex fields and fields that consist of distribution space charges. The relevant field is subdivided into a rectangular or triangular mesh, respectively. The potentials at the node points are solved numerically, take into the boundary conditions [19]. Moreover, this solution is a most outstanding numerical method for solving electric field problems because it involves the discretization of the domain according to the anticipated values of the field distributions, i.e when critical regions, fine mesh generations used (for example, around the tip of rod electrodes), it will save memory space and compute time in the case of complex geometries [23].

Finite Element Discretization

To begin solving the problem, the whole domain is fictional divided into small areas/volumes called elements as shown in Figure 2.9 below. *Nodes* which is unknown throughout the problem domain is approximated in each of these elements in terms of the potential at the vertices. Potential function will be known at the nodes. For some cases of polynomials, it is used for the interpolation of potential inside each element in term of nodal values. Furthermore, the coefficient of this function is represented in terms of unknown nodal potentials. So, interpolation can be directly carried out in terms of nodal values and associated algebraic functions also called as *shape functions*. A lot of elements can be produced through their shape, i.e bar elements in one dimension (1D), quadrilateral and triangular elements in 2D, and hexahedron and tetrahedron elements for 3D problems [2],[17].

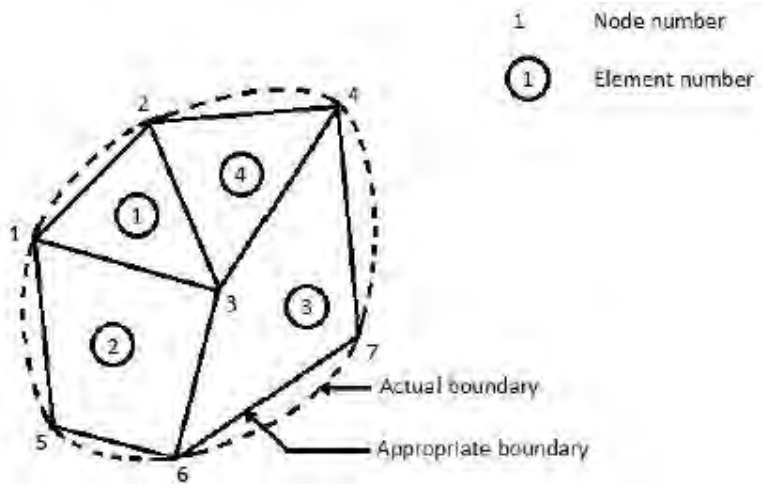

Figure 2.9: A typical finite element division of an irregular domain.

2.6.2 Governing Equations

As the first approximation, the potential V_e with an element is interrelated to other various elements such that the potential is continuous across inter-element boundaries. The exact solution for this problem becomes [2], [17]

$$V(x,y) = \sum_{e=1}^{N} V_e\,(x,y)$$

where N is the number of elements into which the solution region is divided.
A polynomial approximation usually used for the voltage V within an element as in eqn (2.28) while triangular and quadrilateral element equation becomes in eqn (2.29).

$$V_e = (x,y) = a + bx + cy \tag{2.28}$$

$$V_e = (x,y) = a + bx\ + cy\ + dxy \tag{2.29}$$

The potential V_e will becomes zero when it outside the element as quadrilateral elements are non-confirming elements and it will not become zero with element *e* as shown in Figure 2.9. A typical triangular element shown in Figure 2.10.

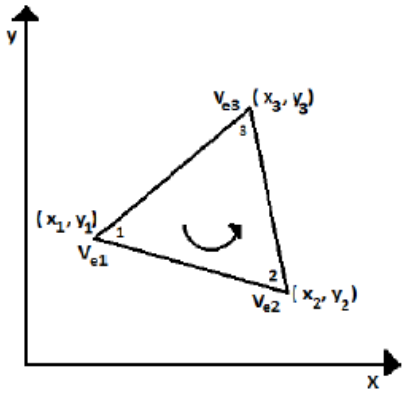

Figure 2.10: Typical triangular element; the local node numbering 1-2-3 must proceed counter clockwise as indicated by the arrow [2].

The potentials V_{e1}, V_{e2} and V_{e3} at nodes 1,2 and 3 are obtained from eqn (2.29).

$$\begin{matrix} V_{e1} \\ V_{e2} \\ V_{e3} \end{matrix} = \begin{bmatrix} 1 & x_1 & y_1 \\ 1 & x_2 & y_2 \\ 1 & x_3 & y_3 \end{bmatrix} \begin{bmatrix} a \\ b \\ c \end{bmatrix} \tag{2.30}$$

The coefficients a, b and c are determined from above equation as

$$\begin{matrix} a \\ b \\ c \end{matrix} \begin{bmatrix} 1 & x_1 & y_1 \\ 1 & x_2 & y_2 \\ 1 & x_3 & y_3 \end{bmatrix}^{-1} \begin{bmatrix} V_{e1} \\ V_{e2} \\ V_{e3} \end{bmatrix} \tag{2.31}$$

Substituting this equation in eqn (2.29), we get

$$V_{e1} = [1 \quad x \quad y\,][1/2A] \tag{2.32}$$

$$\begin{bmatrix} x_2y_2 - x_3y_2 & x_3y_1 - x_1y_3 & x_1y_2 - x_2y_1 \\ y_2 - y_3 & y_3 - y_1 & y_1 - y_2 \\ x_3 - x_2 & x_1 - x_3 & x_2 - x_1 \end{bmatrix} \begin{bmatrix} V_{e1} \\ V_{e2} \\ V_{e3} \end{bmatrix}$$

As the energy per unit length associated with the element e is given by the following equation:

$$W_e = [1/2\varepsilon]\left[\, V_e{}^T\right]\left[C^{(e)}\right][V_e] \tag{2.33}$$

where T denotes the transpose of the matrix

$$[\, V_e\,] = \begin{bmatrix} V_{e1} \\ V_{e2} \\ V_{e3} \end{bmatrix} \tag{2.34}$$

and

$$[C^{(e)}] = \begin{bmatrix} C_{11}^{(e)} & C_{12}^{(e)} & C_{13}^{(e)} \\ C_{21}^{(e)} & C_{22}^{(e)} & C_{23}^{(e)} \\ C_{31}^{(e)} & C_{32}^{(e)} & C_{33}^{(e)} \end{bmatrix} \tag{2.35}$$

2.7 Modelling and Simulation of E_{max} using COMSOL Multiphysics

After the experiment had done, the project is carried out in simulation software. A finite element method is used for the computer simulation. Furthermore, the finite element method, specifically COMSOL Multiphysics is used to carry out the modelling and electric field computations. Figure 2.11 is an example of COMSOL Multiphysics software. It has been widely used in solving engineering problems, such as structural mechanics, heat transfer, fluid flow and acoustics. In order to solve a particular problem, there are three stages involved, which are the pre-processing stage, solving stage, and post-processing stage.

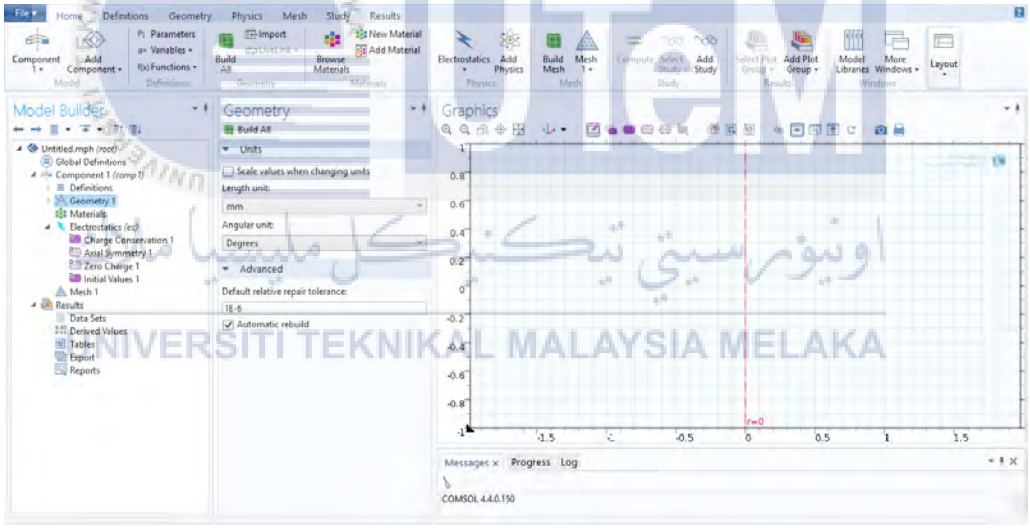

Figure 2.11: An example of COMSOL Multiphysics software.

2.7.1 Finite Element Modelling

For the pre-processing stage, the fundamentals of the model are being determined and developed, such as geometrical structure, selection of materials and properties, domain and boundary conditions, and lastly meshing criteria. For second stage, solving stage, or execution stage, is carried out with a related mathematical model of differential equations, whether the study is time-dependent or stationary. For final stage, post-processing stage, users see the results

and generate a plot for various kinds of variables or parameters, users can choose either a 0D plot, 1D plot, 1D axisymmetric, 2D plot, 2D axisymmetric or 3D plot, depending on the model. The FEM flowchart and the process involved in each stage are shown as Figure 2.12 below.

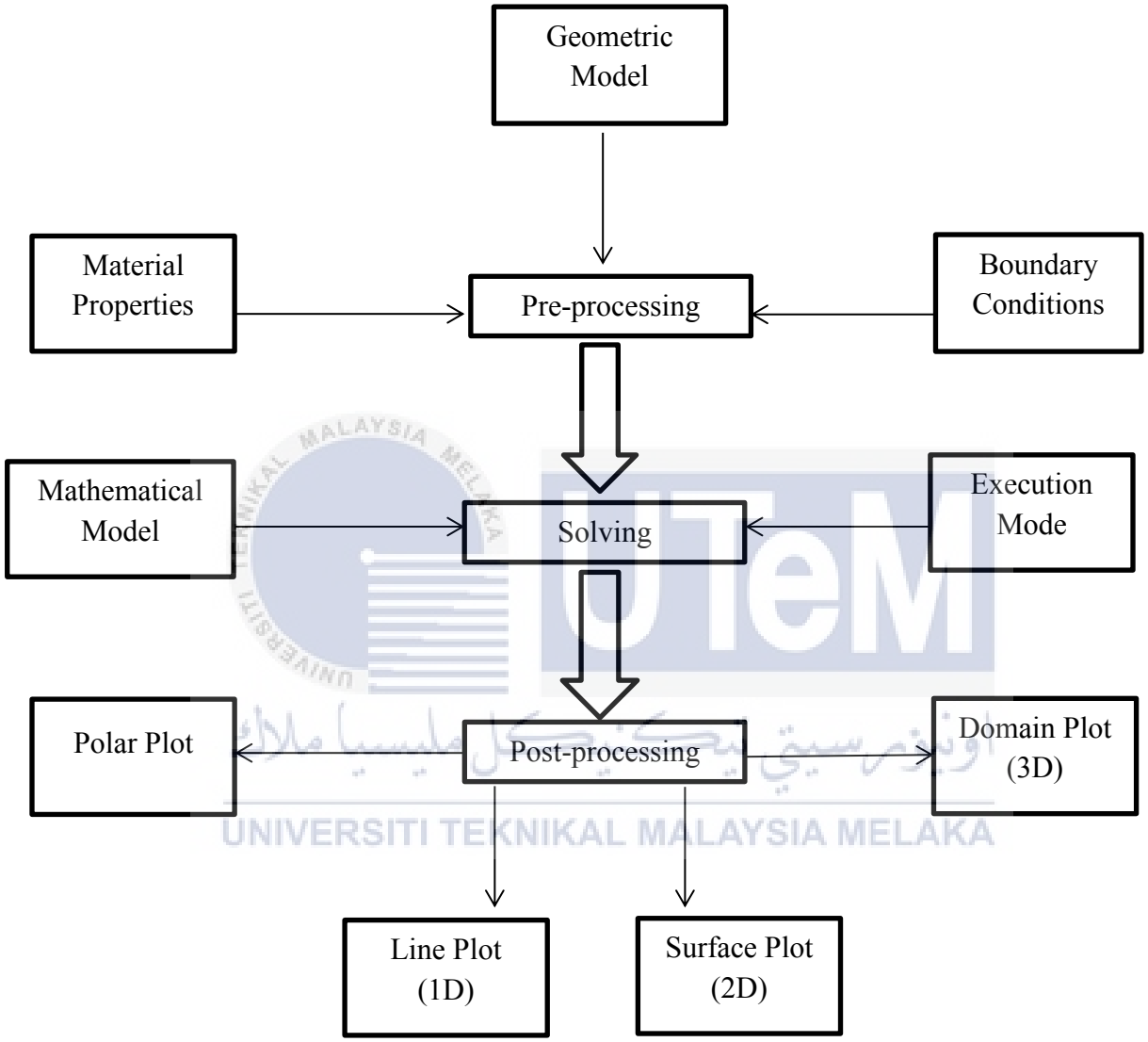

Figure 2.12: General procedures for FEM simulations in COMSOL Multiphysics

2.7.2 Simulated Model

The model of air breakdown is created in the COMSOL Multiphysics software by using a drawing tool that is available. Since the electrodes and pressure vessel are cylindrical in shape, the modelling is simplified into a two-dimensional (2D) model instead of a full-dimensional (3D) model. Even though it is in a 2D model, the accuracy of the simulation results will not be

affected. By follow this technique, memory and processing time will be saved. Based on Figure 2.13 shows an axis-symmetric features are used to simplify further the model without affecting the simulation.

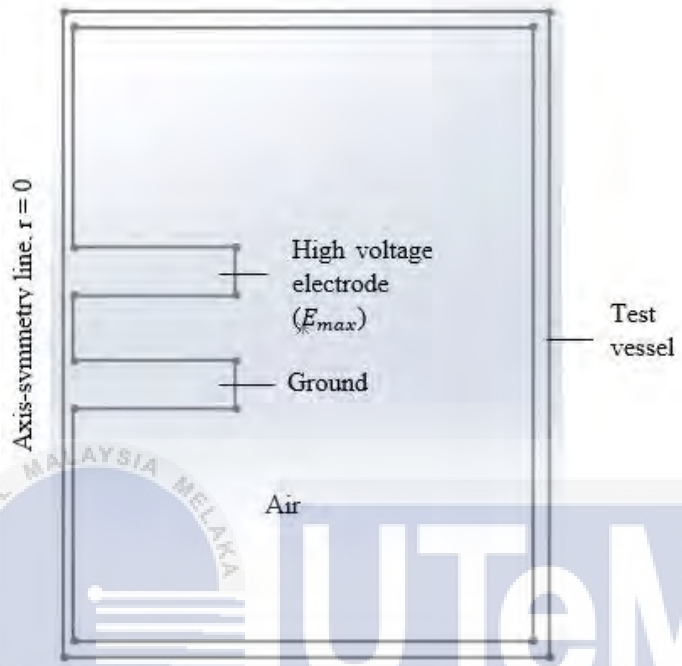

Figure 2.13: A 2D-axis-symmetric model.

Based on the figure above, the model is based on a plane-plane electrode configuration with a gap of 20 mm. As for other electrode configurations with different gaps. The model can be modified to represent the exact test conditions. All the dimensions are scaled according to the actual setup.

2.7.3 Material Properties

In this model, there are three main domains that need to be considered. These are the conductor, conducting rod, electrodes and the dielectric material, i.e. bushing and gas. The conducting domains are defined as what it is in actual test setup, which are steel for the body of the pressure vessel and the rod and brass for electrodes. However, in simulating electrostatic problems, each of conducting domain is excluded in the analysis. There are only external boundaries of those domains are defined which is high voltage terminal or ground. As general, for a vacuum and most non-polar gases, or those known as the inert gases or noble, relative permittivity can be takes as 1, since the number of atoms or molecules per unit volume is very

small compared to those in liquids and solids, except at very high pressure. The material properties used in the modelling, with the exception of conducting materials is shown in Table 2.6 below.

Table 2.6: Properties of materials used for FEM modelling.

Materials	Relative permittivity, ε_r
Air	1.0

2.7.4 Boundary Conditions

In the boundary condition settings, there are only two boundaries in the model have to defined, which is high voltage terminal and ground. For this study, during the experimental phase, the bushing is connected to a high voltage source. The calculated value of U_{50} is then used in the simulation investigation to represent the boundary condition in the high voltage terminal setting and then to plot the corresponding electric field.

0 V or ground is defined for other conducting materials' boundary conditions, i.e. the ground electrode and the ground plane. The symmetry line of the model is then set to be the axial-symmetry axis on the r-z plane.

2.7.5 Mesh

Meshing is the execution mode in solving stage for this COMSOL Multiphysics software. After completing the model with geometric drawing, as well as defining the material properties in the domain section and defining the boundary conditions, the whole model is then disjointed into non-overlapping triangular elements during the meshing process. The triangular elements can be clarified to be smaller resulting in an increase of number meshing elements which depends on the region of interest. Besides, this process used extremely fine mesh and it will enhance the accuracy of the simulation results. In this study, the model was focused on the top of the high voltage electrodes, as it is the most part of maximum electric field magnitudes as can be seen from the concentrated meshing as shown in Figure 2.14. As a result, the mesh refinement can be seen from concentrated meshing which results in reduced element size and the increases number of triangular elements.

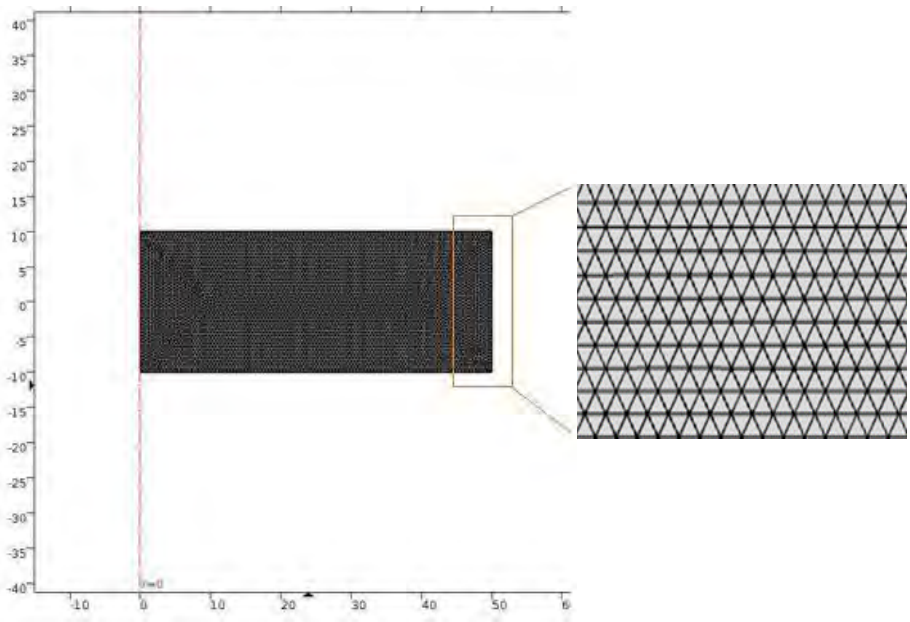

Figure 2.14: Discretization of the domain problem with mesh refinement at the region of interest (plane-plane electrode).

The determination of how far the refinement is needed to trade-off between the accuracy of the plot results, with the memory consumption, and processing time included. As the further refinement of the mesh will result in a smoother plot of the electric field, it will dominate higher computational memory and will take a longer time to process. An enthusiasm refinement will provide short simulation time without deal the accuracy of the results.

2.7.6 Solver Settings

An electrostatic interfaces solver is used in this model and simulated by AC module through COMSOL Multiphysics software. This will allow the user to solve a charge conservation equation for the electric potential given the spatial distribution of the electric charge. Moreover, this interface also give the user to specify permittivity, polarization, or permanent electric displacement of a material to be used in the constitutive relation.

2.8 Summary

In this chapter, an extensive review on the electrical breakdown and electric field stress have been presented. Air is one of the simplest forms of insulator being used in high voltage applications. There are air circuit breakers, air-insulated substations and other equipment. Besides, Finite Element Method (FEM) provides a good solution of Poisson's and Laplace's equations with boundary condition satisfied. There are some numerical techniques have been used in the literature for solving Laplace's and Poisson's equations for the fields between complex electrode arrangement.

CHAPTER 3

RESEARCH METHODOLOGY

3.1 Introduction

This chapter will discuss more detail about the process involved during the project implementation which is illustrated in flowchart. The tests are carried out according to the international BS EN 60060-1 2010 standards. Different topologies are developed to measure the air breakdown voltage, maximum electric field and humidity correction factor by using standard method. To ensure all measurements are valid according to the standard, atmospheric corrections in dry tests have been carried out.

Besides, the project Gantt chart and key milestone are constructed as a timeline towards the completion of this study.

3.2 Flowchart of Project Implementation

Figure 3.1 shows the flowchart of project implementation. There are several steps involves in this study that need to be followed which is starting from power system applications, mechanism of breakdown in gases, simulation of electric fields in uniform and non-uniform field configurations and will end with the analysis and comparison between experiment and simulation results. The explanations for each of the steps will be discussed later. Moreover, in order to use COMSOL Multiphysics software, the user needs to know seven basic processes in Figure 3.2 below. Furthermore, some of the methods or procedures used in this study are related to the previous research that has been done by the previous researchers but with different materials and procedure.

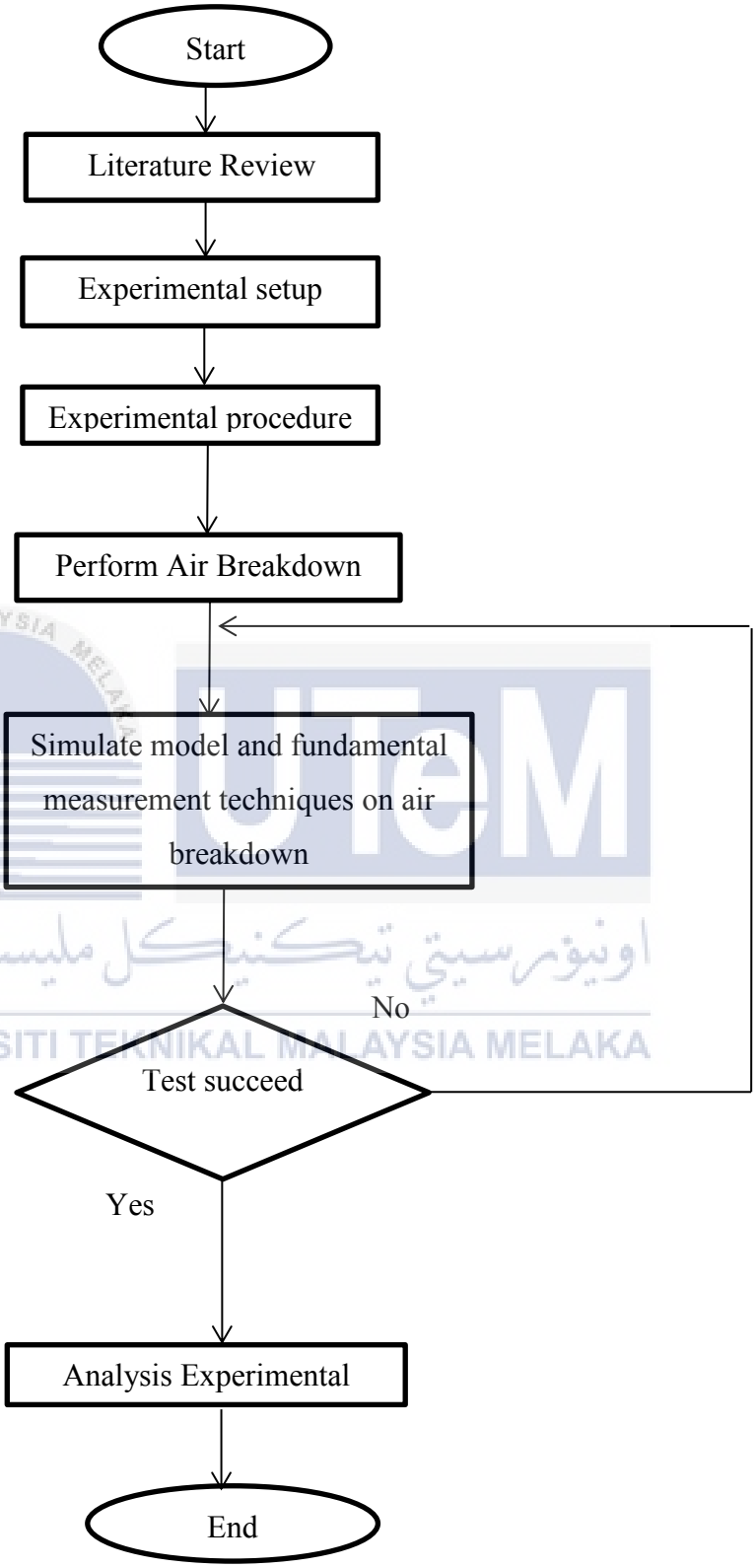

Figure 3.1: Flowchart of project implementation.

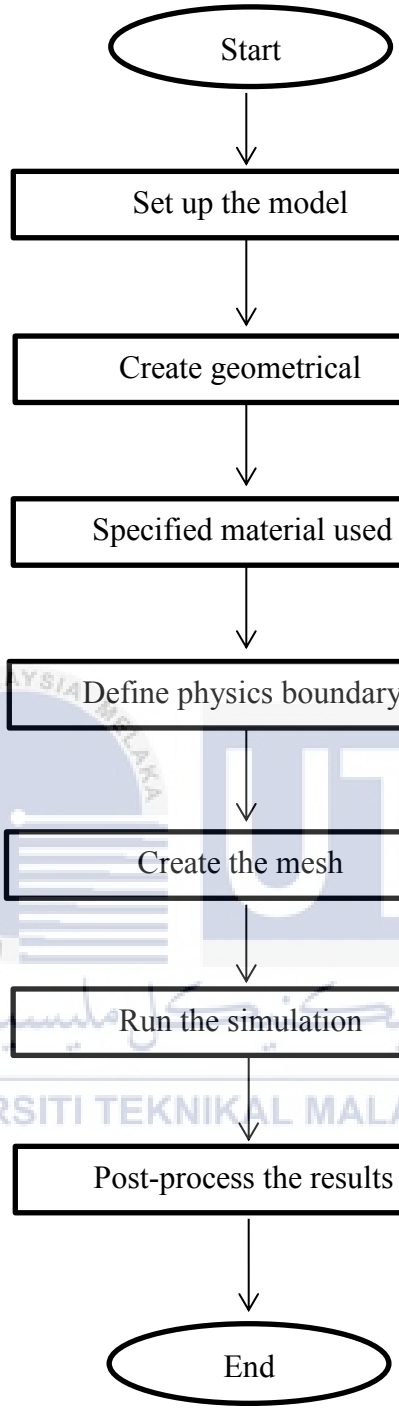

Figure 3.2: Flow chart of seven basics procedures in COMSOL Multiphysics software.

3.3 Literature Review

In this research, a literature review on theoretical of air breakdown mechanism and numerical method for computation of electric field by using different electrodes. The study will focus more on maximum electric field of air breakdown test and simulation of maximum electric field by using COMSOL Multi-physics software. Furthermore, literature will also cover any available standards associated with high voltage testing requirement on gas insulation for RMU design in addition to standard of BS EN 60060-1 2010 (high-voltage test techniques).

3.4 Experimental Setup

There are two main electrode configurations used in this study, namely R6-plane and plane-plane. The plane electrode has a diameter of 100 mm, the R6 electrode has a diameter of 12 mm where both electrodes are made of brass metal and air is acting as an insulating medium between these electrodes as shown in Figure 3.3. In this particular study, R6 electrode is under high voltage grade, all the test device is prepared in the laboratory and its schematic diagram is constructed shown in Figure 3.3. The lower plane electrode which is above the ground plane is grounded where as the top rod electrode is connected with HV connector. According to Figure 3.4 shows a custom made test vessel that will be used in this project. It is the courtesy of Indkom Engineering Sdn. Bhd. Furthermore, the vessel must undergo some precaution test before it can be used such safety measures and capability of the vessel to withstand high pressure, gas leak test, high voltage withstand test and also functionality of the attached instrument devices. Figure 3.5 shows a connection test vessel with high voltage equipment. This vessel was designed to withstand up to 40 kV supply AC voltage and has volume capacity of 205 litre.

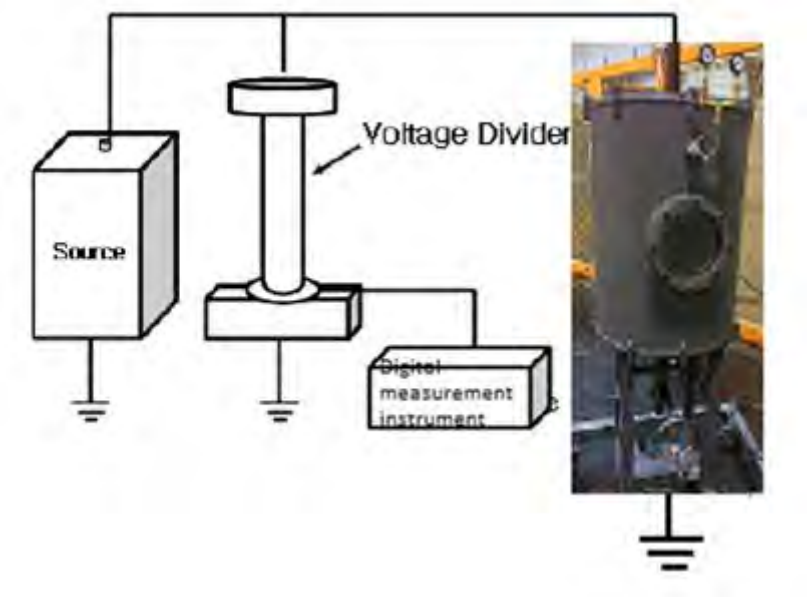

Figure 3.3: The schematic diagram of air breakdown voltage test.

Figure 3.4: Custom made test vessel with the courtesy of Indkom Engineering Sdn. Bhd. (volume capacity = 205 litre and withstand voltage = 40kV AC).

Figure 3.5: The connection of test vessel with high voltage equipment.

The voltage level can be controlled manually by using AC Controller, Operating Terminal (OT) 276. This equipment is very easy to control an AC test system as depicted in Figure 3.6 while Figure 3.7 shows Digital Measuring Instrument as AC System Controller which allows comfortable, flexible automated control of an AC system.

Figure 3.6: AC Controller

Figure 3.7: Digital Measuring Instrument

3.5 Experimental Procedure

In this project, a series of breakdown strength test was conducted by using AC voltages (power frequency) and the test should be compliance with the required standard, i.e. BS EN 60060-1 2010 or other related standard. This project will follow class 3 of progressive stress tests [24] in Annex A. In a Class 3, a procedure that always dominant to a disruptive discharge on the test object is applied n times. The test may be rise constantly or in steps until a disruptive discharge occurs at a voltage U_i or held constant at a level until a disruptive discharge at time t_i is noticed. Most of the discharge occurred at ($n > 10$). There is such test with continuously or stepwise increased direct and alternating or stepwise increased impulse voltages. But tests with interrupt discharges happened on the front of an impulse fall into this class as in Figure 3.8 [24].

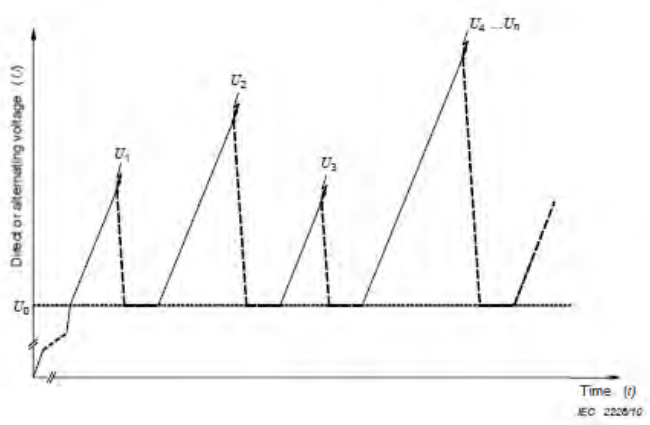

Figure 3.8: Continuous voltage increase [24].

A minimum of 50 measurements on each experiment will be taken for the purpose of statistical analysis. This experiment performs in order to determine the maximum electric field between different electrodes by use air. The electrodes of brass metal are used in this experiment, which is located in the sealing chamber. Gap distance can be adjusted from the outside of the sealing chamber with the adjustment as well pressure of 1 atmosphere as shown in Table 3.1 below.

Table 3.1 : Gap distance to be tested.

	Plane-Plane Electrode (mm)	Rod-plane Electrode (mm)
1	5	10
2	10	20
3	15	30
4	20	40
5	-	50

3.6 Perform AC Air Breakdown Test

To determine the AC breakdown voltage, the test voltage is slowly increasing until it reached critical value and breakdown voltage will formed with the validation test of 50 times. The experiment will be set in one minute and reset again. All the same steps were repeated again. 50% disruptive discharge voltage of a test object is used to determine to ensure all measurements are valid according to the standard. U_{50} is prospective voltage value which has a 50 % probability of producing a disruptive discharge on the test object [24]. For this experiment, U_{50} is the mean values for 50 breakdown voltage data. Digital measuring instrument is used to record the breakdown voltage.

3.7 Modelling and Simulation of E_{max} using COMSOL Multiphysics software

There are the steps for modeling and simulation can be summarized using the flow chart in Figure 3.9 below:

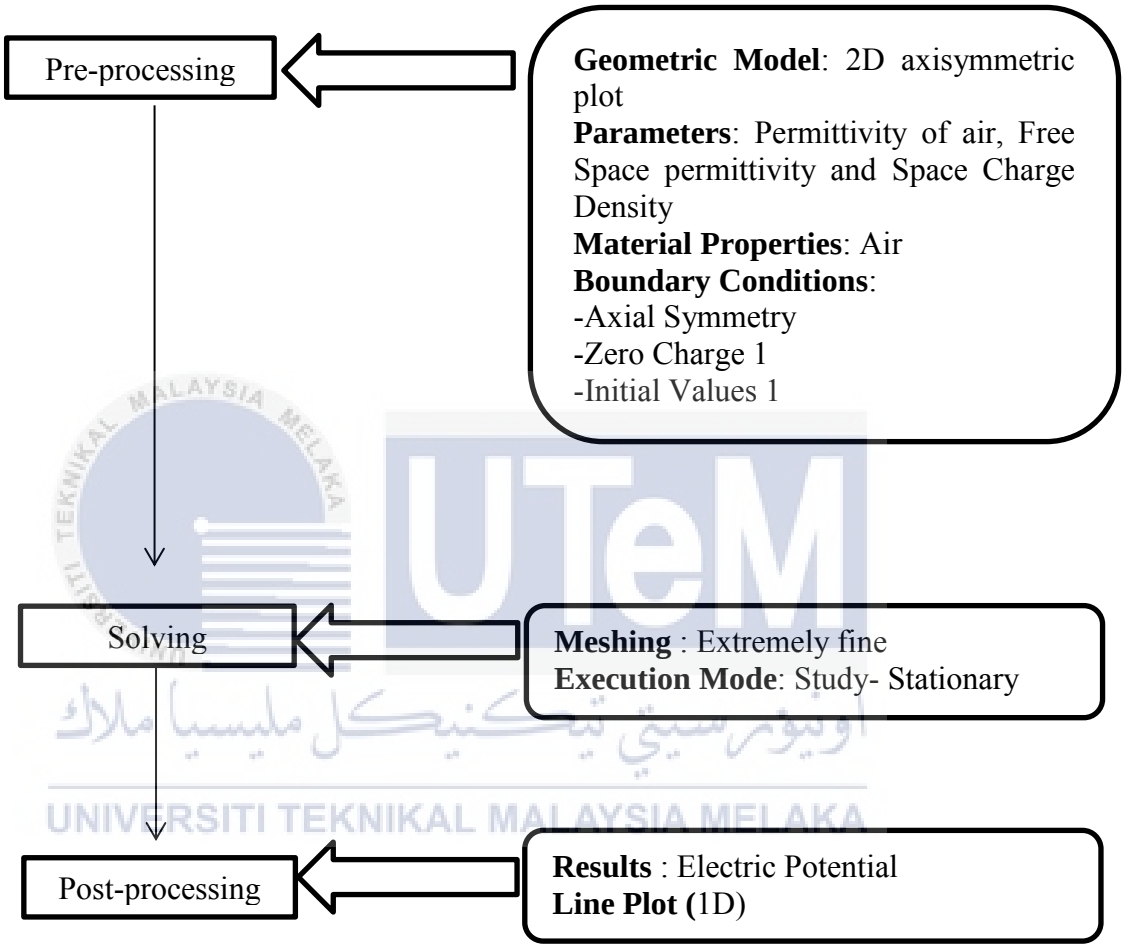

Figure 3.9: The summarize of flow chart for modelling and simulation using COMSOL Multiphysics software.

3.8 Fundamental Measurement Techniques on Air Breakdown

3.8.1 Atmospheric Corrections in Dry Tests

Due to the possibility of degradation with repeated voltage applications, and in order to ensure all the tests meet the national standard, it is fairly important to consider correction factors for each test condition. The standard reference atmosphere is taken as

temperature t_0 = 20℃

absolute pressure p_0 = 1013hPa (1013 mbar)

absolute humidity h_0= 11 g/m^3

This section will explain atmospheric correction factors related to this study as stated in.

3.8.2 Atmospheric Correction Factors for Air Gaps

Based on these standard also, the breakdown of air insulation depends on the atmospheric conditions. It is usually increased with air density or humidity. When the relative humidity exceeds 80%, the breakdown voltage may become irregular. Hence, the breakdown voltage is proportional to the atmospheric correction factor K_t below

$$K_t = k_1 k_2 \tag{3.1}$$

where

k_1: is the air density correction factor

k_2: the humidity correction factor

By applying correction factors, a breakdown voltage measured, *U* in given test conditions under temperature *t*, pressure *p*, and humidity *h*, is then converted to the value U_0 which would have been obtained under standard atmospheric conditions with a relation of

$$U_0 = U/K_t \tag{3.2}$$

3.8.3 Air Density Correction Factor, k_1

In addition, the air density correction factor k_1 depends on the relative air density δ and can be expressed as

$$k_1 = \delta^m \tag{3.3}$$

where *m* is an exponent given in Table 3.2.

If the temperatures, i.e. *t* and t_0 are expressed in degrees Celsius, and the pressures (i.e. *p* and p_0) are expressed in the same units, the relative air density is represented by

$$\delta = \frac{p}{p_0} \times \frac{273 + t_0}{273 + t} \tag{3.4}$$

The above correction is considered reliable for $0.8 < k_1 < 1.05$.

3.8.4 Humidity Correction Factor, k_2

Besides that, the humidity correction factor is represented by

$$k_2 = k^w \tag{3.5}$$

where *w* is an exponent given in Table 3.2.

For an AC breakdown, *k* is a function of the ratio of absolute humidity, *h* to the relative air density, and δ is given by

$$k = 1 + 0.012(h/\delta - 11) \qquad \text{for } 1\ g/m^3 < h/\delta < 20\ g/m^3 \tag{3.6}$$

3.8.5 Exponents *m* and *w*

Since the correction factors depend on the pre-discharges, a parameter, *g*, can be illustrated as shown below

$$g = \frac{U_{50}}{500L\delta k} \tag{3.7}$$

where

U_{50}: 50% breakdown voltage at the actual atmospheric conditions (kV)

L: minimum discharge path (m)

δ: relative air density

k: dimension less parameter

In a case where U_{50} is not available, it can be assumed to be 1, 1 times the test voltage U_0. For specified range of *g*, the exponents *m* and *w* can be obtained from Table 3.2.

Table 3.2: Values for exponent *m* for air density correction and *w* for humidity correction, as a function of the parameter *g*.

g	***m***	***w***
< 0.2	0	0
0.2 to 1.0	*g*(*g*-0.2)/0.8	*g*(*g*-0.2)/0.8
1.0 to 1.2	1.0	1.0
1.2 to 2.0	1.0	(2.2 – *g*)(2.0-*g*)/0.8
>2.0	1.0	0

3.8.6 Humidity Measurement for Correction

In this study, the data of temperature and humidity measurements are recorded in relative humidity and degrees Celsius. The relation between the absolute humidity, *h*, with the relative humidity and the ambient temperature is recorded as

$$h = \frac{6.11 \times R \times e^{\frac{17.6 \times t}{243 \times t}}}{0.4615 \times (273 + t)} \tag{3.8}$$

where

h: the absolute humidity in g/m^3

R: the relative humidity in percent

t: the ambient temperature in ˚C

The steps for atmospheric corrections can be summarized using the flow chart in Figure 3.10 below:

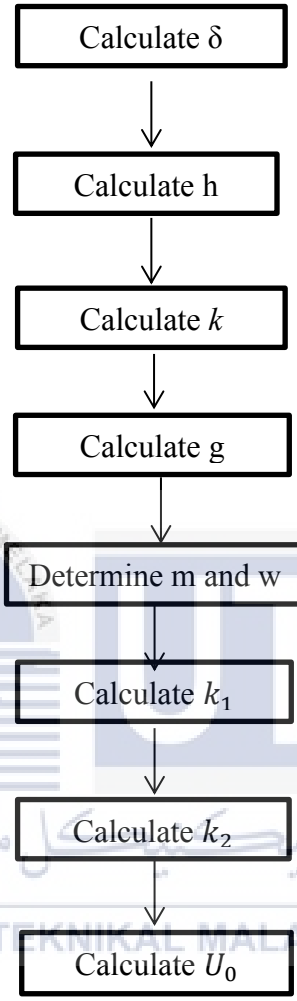

Figure 3.10: Flowchart for atmospheric corrections in dry tests.

3.9 Analysis Experimental Results

After gathering all the data and information from the experiment and simulation, the analysis has been carried out. Air breakdown voltage and maximum electric field can be determined based on data analysis and simulation result. According to the experimental results, the relationship between the different electrodes configurations and gap distance in 1 atmospheric pressure will be discussed more details in Chapter 4.

3.10 Summary

Overall, the maximum electric field and air breakdown voltage can be determined in this project. Besides, the experiment is conducted with other constant parameter such as pressure, gap length and electrode configurations for a total of 50 tests experiment. Meanwhile, the test is complied with the required standard of BS EN 60060-1 2010. Lastly, all the experiment results will be compared with the modelling of geometry using COMSOL Multiphysics software. Next chapter will present the results and discussion obtained based on the experiments that have been done.

CHAPTER 4

RESULTS AND DISCUSSION

4.1 Introduction

This chapter presents the results and analysis of research work that have been done in Chapter 3 based on the experiment and simulation results in order to fulfil the objectives of this study.

4.2 Effect of Pressure, Temperature and Humidity

In the experiment, the model in Figure 4.1 has been selected in order to investigate the effects of pressure, temperature and humidity on the breakdown behaviour of air which have been analysed with diameter of 100 mm for plane electrode for 50 times test. Furthermore, the test was used constant pressure which is 1 atm. The value of U_{50} before and after correction were shown in Table 4.1.

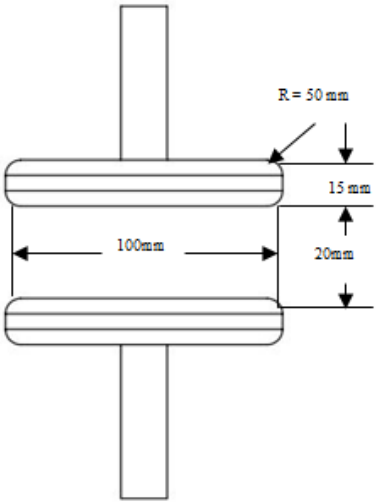

Figure 4.1: The model of plane-plane electrode configuration.

The value of E_{max} for uniform field configuration was calculated by using the formula as

$$E_{max} = \frac{V}{d} \tag{4.1}$$

Furthermore, the evolution error of U_{50} and E_{max} before and after correction can be calculated by equation 4.2 below

$$Error(\%) = \frac{|\ After\ correction - Before\ correction\ |}{|\ After\ correction\ |} \times 100\% \tag{4.2}$$

Table 4.1: U_{50} and E_{max} values in plane-plane electrode configuration during before and after correction.

Air gap distance (mm)	Temperature (℃)	Humidity, RH (%)	Before correction		After correction		Error of U_{50} (%)	Error of E_{max} (%)
			U_{50} (kV)	E_{max} (kV/mm)	U_{50} (kV)	E_{max} (kV/m)		
5	30	82	14.52	2.90	15.21	3.04	4.54	4.61
10	28.9	82	19.84	1.98	20.71	2.07	4.20	4.35
15	29.8	82	29.48	1.97	30.86	2.06	4.47	4.37
20	29.4	82	34.78	1.74	36.36	1.82	4.35	4.40

As depicted in Table 4.1, constant pressure and humidity were used in these experiment and temperature recorded were difference for each gap length. The analysis cannot be in details as temperature and gap lengths are not constant. The error of U_{50} and E_{max} before and after correction were depends on temperature and humidity reading during the experiment. The range of error in between 4.20 % until 4.54 % for U_{50} and 4.35 % until 4.61 % for E_{max}. This verified the data of plane-plane electrode configuration between measured and calculated data.

Figure 4.2 shows the U_{50} for air breakdown for these experiment during before and after correction. In addition, the maximum electric field was noted and plotted against gap distance by varying the gap distance between the electrodes as depicted in Figure 4.3.

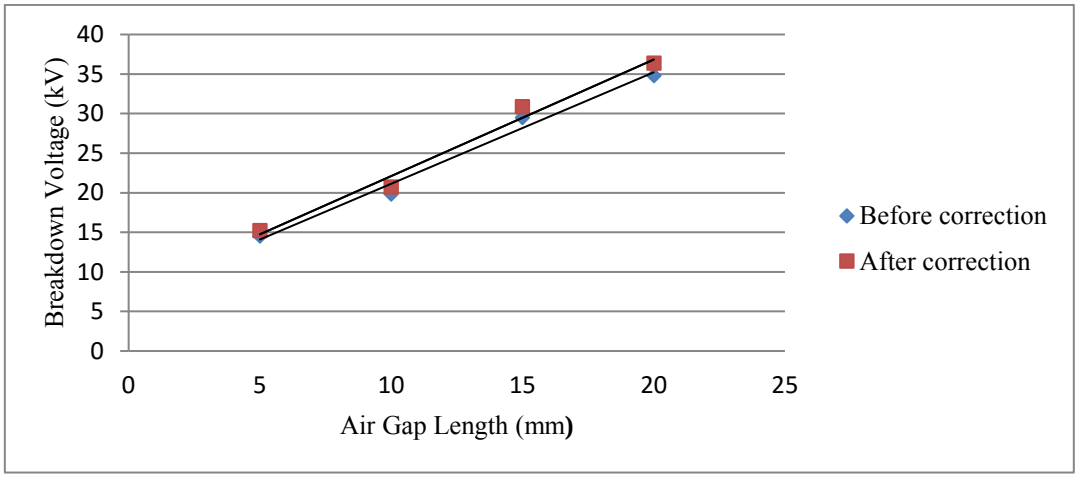

Figure 4.2 : U_{50} for air breakdown in plane-plane gap length before and after correction.

For uniform field configuration, the graph of U_{50} approximately linear for both correction when humidity recorded was 82 % and it remain constant from 5 mm until 20 mm. As depicted in Figure 4.2, the value of U_{50} was increases after correction even though temperature was changes from 28.9℃ until 30℃. The calculation techniques of U_{50} after correction can be used based on eqn (3.1) until (3.8) in Chapter 3.

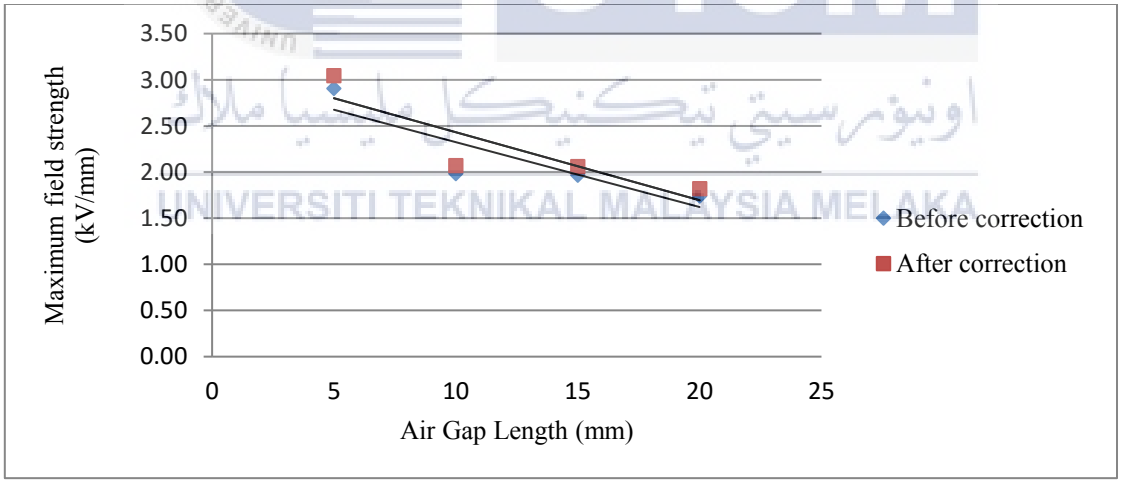

Figure 4.3: E_{max} for air breakdown in plane-plane gap length before and after correction.

Figure 4.3 indicates that the graph of E_{max} decreasing linearly except for E_{max} during 10 mm air gap length for both correction when humidity recorded was 82 % and it remain constant from 5 mm until 20 mm. It is obvious that most of maximum electric field occured

between 1.74 up to 3.04 kV/mm. As depicted in Figure 4.2, the value of E_{max} was decreases after correction even though temperature was changes from 28.9℃ until 30℃.

Further tests have been carried out by using rod-plane electrode configuration as shown in Figure 4.4 in order to study the same task. The models which have been analysed with diameter of 12 mm for rod and 100 mm for plane electrode. Based on Table 4.2 shows the values of U_{50} and E_{max} for air breakdown on rod-plane electrode before and after correction.

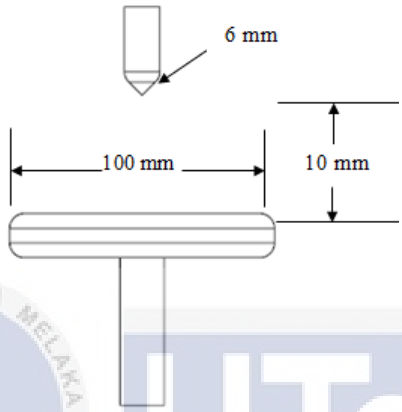

Figure 4.4: The model of rod-plane electrode configuration.

The value of E_{max} can be find by using formula given by H. Javadi [25] as shown in eqn (4.3).

$$E_{max} = \frac{2V}{r \ln(\frac{4d}{r})} \quad (4.3)$$

where

V = the applied voltage (kV)

d = gap length (mm)

r = radius (mm)

while the evolution error of U_{50} and E_{max} before and after correction can be determined by eqn (4.2) above.

Table 4.2: U_{50} and E_{max} values in rod-plane electrode configuration during before and after correction.

Air gap distance (mm)	Temperature (°C)	Humidity, RH (%)	Before correction		After correction		Error of U_{50} (%)	Error of E_{max} (%)
			U_{50} (kV)	E_{max} (kV/mm)	U_{50} (kV)	E_{max} (kV/m)		
10	28.2	82	15.73	2.76	16.38	2.88	3.97	4.17
20	29.3	77	17.89	2.30	18.02	2.32	0.72	0.86
30	29.3	77	20.41	2.27	18.79	2.09	7.94	7.93
40	29.2	77	22.30	2.26	20.31	2.06	8.92	8.85
50	30.1	76	23.10	2.20	21.61	2.05	6.45	6.82

As illustrated in Table 4.2, the experiment conducted with a constant pressure but difference temperature and humidity reading. The analysis cannot be in details as temperature, humidity and gap lengths are not constant. Therefore, the parameters influenced the error of U_{50} and E_{max} before and after correction. Therefore, the range of error for U_{50} in between 0.72 % until 8.92 % while error for E_{max} started from 0.86 % until 8.85 %. This can validated the date of rod-plane electrode configuration between measured and calculated data. The value of U_{50} for air breakdown used in these experiment were shown in Figure 4.5 before and after correction. This is because the majority of insulating systems are in and non-uniform gap configurations. In addition, the electric field distribution and maximum electric field were noted and plotted against gap distance by varying the gap distance between rod-plane electrode were shown in Figure 4.6.

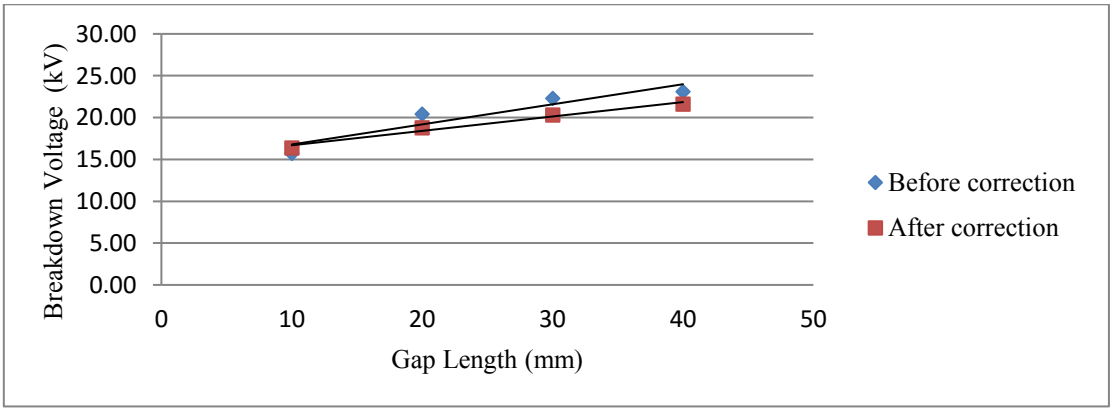

Figure 4.5: U_{50} for air breakdown in rod-plane gap before and after correction.

Referring to Figure 4.5, as expected under non-uniform field configuration, the graph of U_{50} almost linear for both correction when humidity recorded were 76 until 82 % from 10 mm until 50 mm. However, the values of U_{50} was slightly decreases after correction when temperature was changes from 28.2℃ until 30.1℃. Earlier studies in breakdown voltage has been carried out by Ekram [26], as humidity increases, rod-gap breakdown voltage increases linearly.

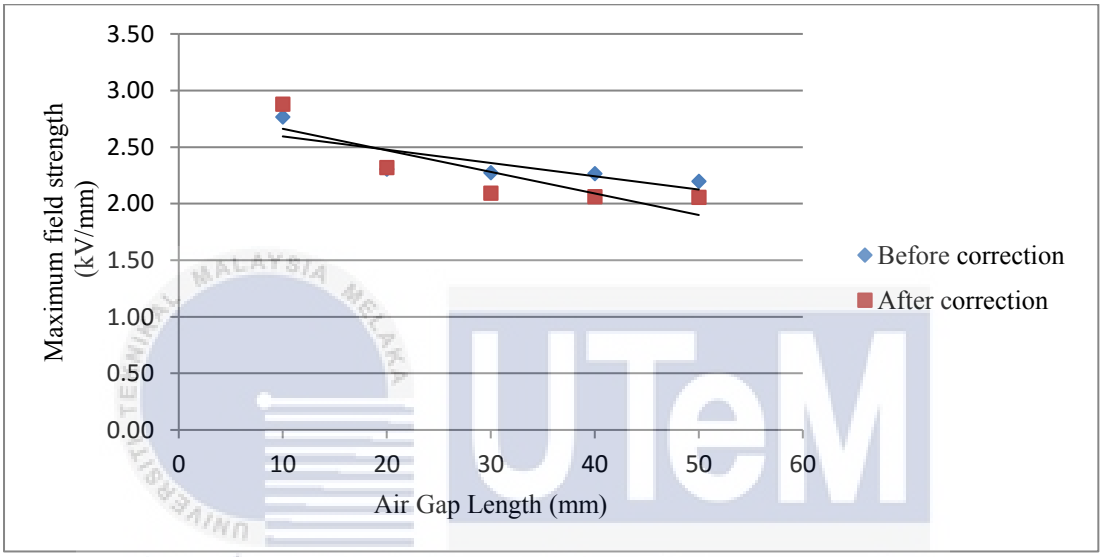

Figure 4.6: E_{max} for air breakdown in rod-plane gap length during before and after correction.

Closer examination of the Figure 4.6 above, most of maximum electric field occurred between 2.05 up to 2.88 kV/mm. The graph of E_{max} for both correction does not linear along the line and it was slightly decrease after correction. There was an investigation on effect of humidity on the breakdown characteristics has been carried out by D. Rodriguez [27] as humidity is the amount of water vapour in air and it depends on many factors such as geographical location, ambient temperature, wind and atmospheric pressure. It can be described in several ways while based on an investigation proposed by Li Ming [28] with study of humidity effects on dielectric strength, it shown that the increase rate of breakdown voltage with humidity for the rod-plane air gaps is a typical value resulting from a positive streamer controlled breakdown process [28].

For non-uniform field configurations and dc voltages, the humidity effect is dependent on the polarity of the electrodes. For the case when the energized electrode is negatively

charged, the variation of the breakdown voltage with humidity is negligible. When refer to the atmospheric correction in dry tests, the breakdown voltage is to be higher as increases in humidity. Moreover, it is noteworthy that the effect of humidity correction factor, k_2 is greater as the gap distance increased [5]. The distance traversed by the ions subject to the electric field decreases with increasing gap length. For longer gap lengths, the electric field strength is reduced making the drift velocity of the ions slower [27]. As for rod-plane gap length, the breakdown voltages increased with humidity as resulting from a positive streamer controlled breakdown process [28].

4.3 Effect of Gap Length

As seen in experimental results for uniform field configuration in Figure 4.2, by considering only U_{50} after correction factor, the value of U_{50} increased by 1.36 times for 10 mm gap, 2.03 times for 15 mm gap and 2.39 times for 20 mm gap. This shows that a bigger gap length in electrode configuration will introduce a slightly bigger increase in U_{50} with the pressure of 1 atm. Furthermore, there are only small differences occur between U_{50} before and after correction. The values of U_{50} were increased approximately linearly with the pressure of 1 atm. For 10 mm, the value of U_{50} was 19.84 kV before correction and it increases slightly to 20.71 kV after correction. The highest value of U_{50} before correction was 34.78 kV and it rises sharply to 36.36 kV after correction for 20 mm gap length.

Closer consideration of the E_{max} curves for uniform field configuration in Figure 4.3 offers a clear indication that, the E_{max} values are almost the same for every gap length except for 10 mm air gap length. As U_{50} is increased, the ability of air to withstand E_{max} (and high stress) is decreased before and after correction. Moreover, various factors that affect the dielectric strength of air was influenced by atmospheric conditions and humidity [29]. The air density like temperature and pressure can affect the data results of experiments.

By considering after correction for non-uniform field configuration, the value of U_{50} in Figure 4.5 increased by 1.10 times for 20 mm gap, 1.15 times for 30 mm gap, 1.24 times for 40 mm gap and 1.32 times for 50 mm gap. This shows that a bigger gap length in electrode configuration will introduce a slightly bigger increase in U_{50} with the pressure of 1 atm. Furthermore, there are only small differences exist between U_{50} before and after correction.

The graph of U_{50} was increased almost linearly with the pressure of 1 atm. The value of 10 mm for U_{50} before correction was 15.73 kV while after correction U_{50} was increased up to 16.38 kV. Because of short rod plane gap length, the electrodes is similar to uniform field, there is no discontinuity in the breakdown voltage pressure characteristics for short electrode gap [3].

For non-uniform field configuration in Figure 4.6, the E_{max} curves offers a clear indication that, the E_{max} values are almost the same for every gap length. As U_{50} is increased, the ability of air to withstand E_{max} (and high stress) is decreased before and after correction factor. Moreover, various factors that affect the dielectric strength of air is influenced by atmospheric conditions and humidity [29]. The air density like temperature and pressure can affect the data results of experiments.

4.4 Simulation of Maximum Electric Field, E_{max}

The values of U_{50} after correction in Table 4.1 were used in the COMSOL Multiphysics software to compute the output of E_{max} while Table 4.3 shows result of E_{max} in each test configuration.

Table 4.3: E_{max} values of breakdown voltage by using COMSOL Multiphysics software.

Air gap length (mm)	Maximum electric field, E_{max} (kV/mm)
5	3.04
10	2.05
15	2.03
20	1.80

Based on Table 4.3, the highest value of E_{max} occurred at 3.04 kV/mm with voltage of 15.21 kV during 5 mm air gap length while the value of E_{max} approximately at 1.80 kV/mm for a voltage of 36.36 kV during 20 mm air gap length. The parameter likes pressure, temperature and humidity were neglected when simulating this geometry.

As illustrated in Figure 4.7 shows the model geometry simulated with parameter defined (see Appendix D) as the electric field distribution along axis for 20 mm gap length plane-plane

field configuration was observed in Figure 4.8. It is shows that the field strength is same along the y-axis. In addition, the results of E_{max} by simulation was shown in Figure 4.9.

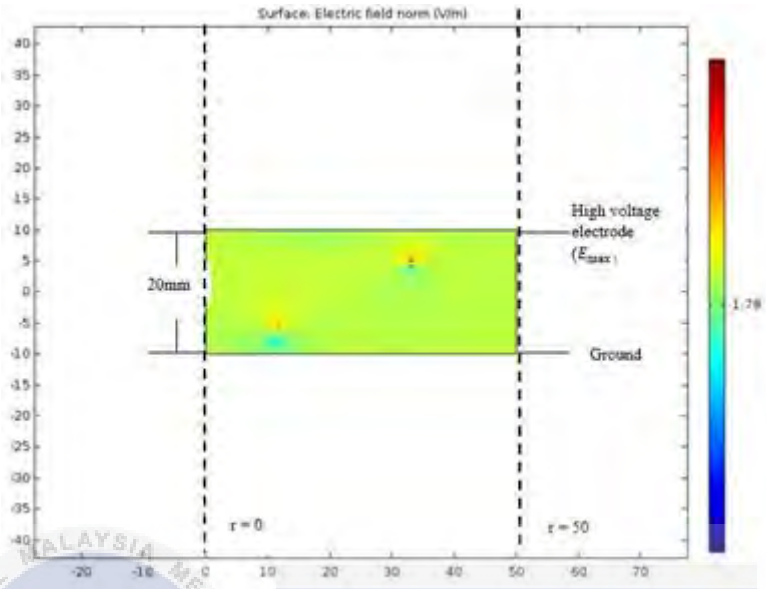

Figure 4.7 : The model geometry stimulated of 20 mm air gap.

Figure 4.8 : Electric field along the gap of the plane-plane gap electrode (refer to Figure 4.7).

Referring to Figure 4.7, the colour table range shows how the electric field varies inside the geometry. Red colour was defined as the highest electric field while dark blue colour was stated as the lowest electric field distribution along the axis for each geometry. In addition, green colour was defined as the maximum electric field occurred inside the geometry but there are some instability of electric field

The line graph of electric field for plane-plane field configuration in Figure 4.8 was straight line along the geometry and it proven for other gap length. Furthermore, E_{max} was present a very high stress region and eventually pre-discharge began to occur [7]. The air breakdown happened at the top of high voltage electrode until the surface of the ground electrode. The results of E_{max} simulation was shown in Figure 4.9.

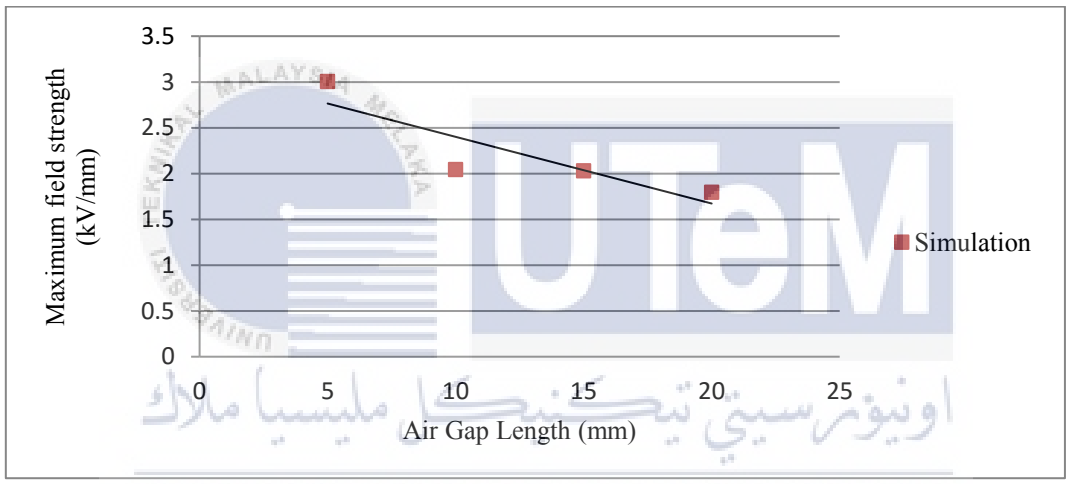

Figure 4.9 : E_{max} values in plane-plane configuration by calculation and simulation.

Based on the E_{max} curves (see Figure 4.9), the graph of E_{max} values decreasing linearly when simulate from 5 until 20 mm air gap length. As the gap length is increased, the ability of air to withstand E_{max} (and high stress) is decreased. This is particularly true for a higher gap length between the electrodes. Also, importantly, it can be deducted that same amount of air pressure, a lower E_{max} withstand capability can be achieved in a longer gap length for this particular electrode configuration.

The simulation was continued with simulation of rod-plane field configuration and the results of E_{max} were shown in each test configuration in Table 4.4 below.

Table 4.4: E_{max} values of breakdown voltage by using COMSOL Multiphysics software.

Air gap distance (mm)	Maximum electric field of breakdown voltage (kV/mm)
10	3.10
20	2.50
30	2.10
40	2.00
50	1.98

As depicted in Table 4.3, the highest value of E_{max} occurred at 3.10 kV/mm with a voltage of 16.38 kV during 10 mm air gap length while the lowest value of E_{max} occurred at 1.98 kV/mm for a voltage of 21.61 kV during 20 mm air gap length. The parameter likes pressure, temperature and humidity were also abandoned when simulating the geometry.

Figure 4.10 shows the model geometry simulated while field strength distribution along axis for 10 mm gap rod-plane electrode configuration was observed in Figure 4.11. Besides, the results of E_{max} for gap length between 10 until 50 mm was shown in Figure 4.12.

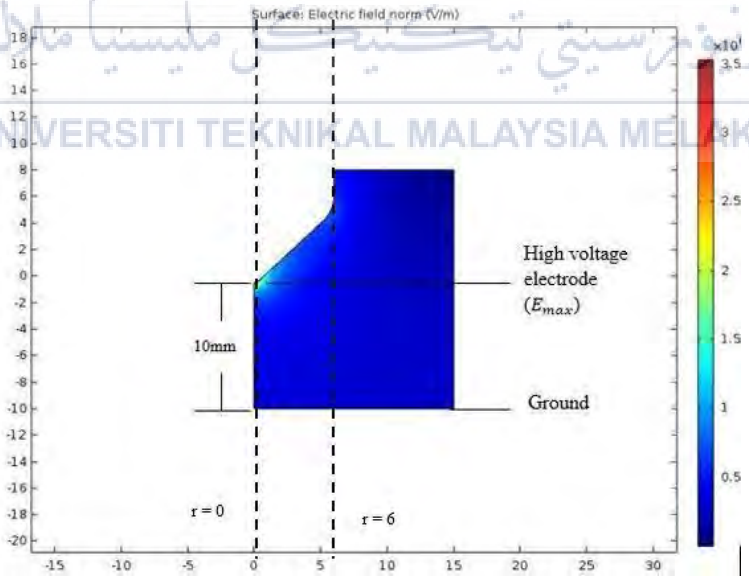

Figure 4.10: The model geometry was simulate using COMSOL Multiphysics software of 10 mm air gap.

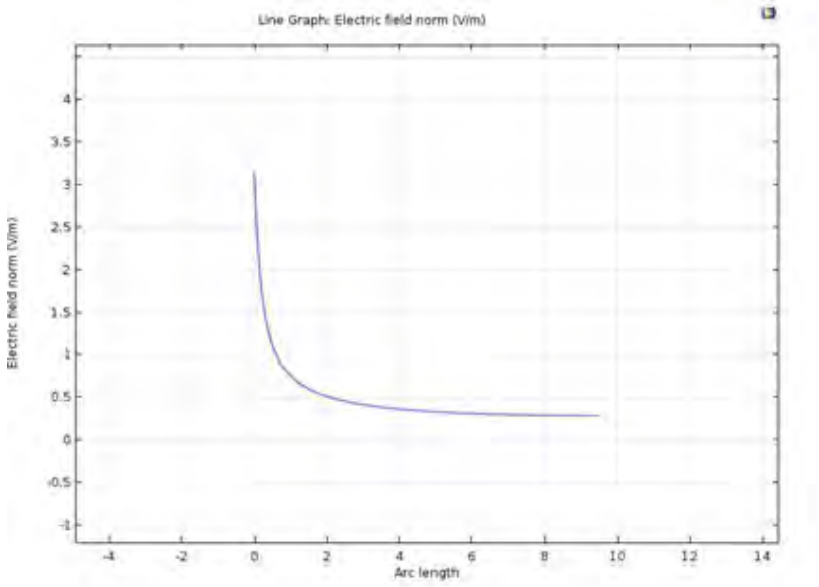

Figure 4.11: The field strength along axis for 10 mm air gap length of rod-plane electrode configuration.

As clearly in Figure 4.10, the magnitude of the electric strength is represented by colour shades. Red colour indicated the highest maximum electric field while dark blue colour defined as lowest electric field inside the geometry. As expected, E_{max} occurred at the tip of the rod which is right on the central longitudinal axis of the rod with light blue color shades. It is most likely location where the pre-discharges will occur and followed by air breakdown while other part was distributed with low electric field (dark blue colour).

Figure 4.11 shows the line graph of electric field decreasing from 3.1 kV/mm to 0.3 kV/mm and it became saturated after 2 mm air gap length. The output of graph were proven while simulating for other air gap length geometry. The simulation has been carried out to obtain E_{max} curves for 10 mm until 50 mm gap length as shown in Figure 4.12.

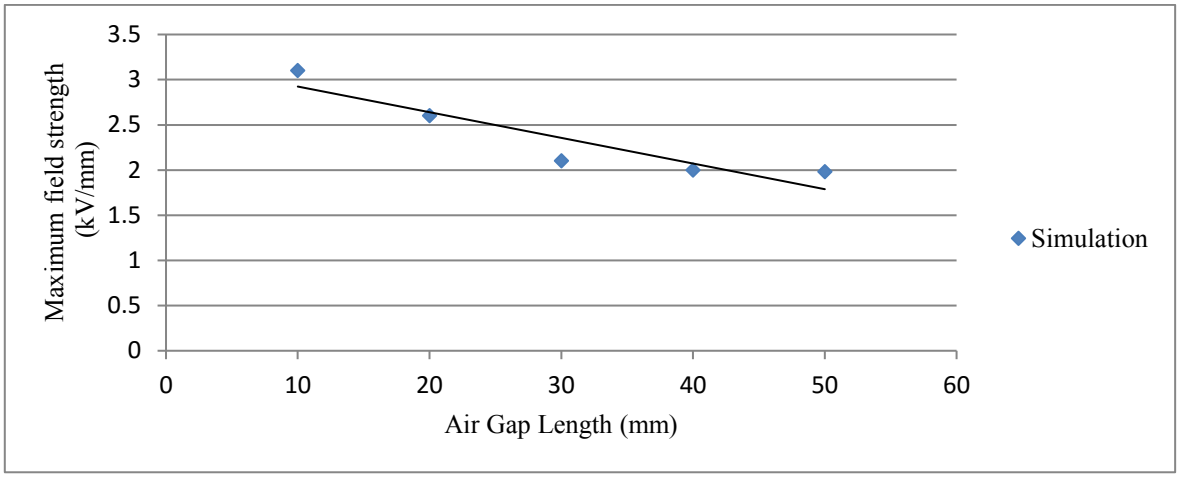

Figure 4.12: E_{max} values in rod-plane configuration by calculation and simulation.

Based on the E_{max} curves (see Figure 4.12), the graph of E_{max} values decreasing linearly when simulate from 10 until 50 mm air gap length. Besides, the values of E_{max} decreased as the air gap length increased. It has to be recognized that E_{max} values are purely simulation, as they are not real electric field. This is due to the fact that breakdown happens just before the electric field reaches the calculated E_{max} values [7]. It also depends mainly on the rod radius and changes slightly with the gap length. The average field strength was sharp drop in the maximum electric field but it gradually decreases in the gap length.

It is desirable to calculate the field utilization factor, η for each electrode configuration by using eqn. (2.26) as the concept of non-uniformity can be proven by value of field utilization factor for a better understanding, i.e a higher value of η represents a more uniform electric field and E_{mean} can be calculated using eqn (2.25) while E_{max} were calculated using formula given in eqn (4.1). The utilization factor, η, for each electrode configuration is shown in Table 4.5.

Table 4.5: Field utilization factors for each electrode configuration.

Electrode configuration	Air Gap (mm)	E_{mean} (kV/mm)	E_{max} (kV/mm)	Field utilization factor, η
Rod-Plane	10	1.64	2.88	0.57
	20	0.90	2.32	0.39
Plane-Plane	10	2.07	2.07	1
	20	1.82	1.82	1

Based on Table 4.5, it clearly that the η was highest which is 0.57 when 10 mm for rod-plane, while plane-plane electrode configuration, the values of the η was 1 for both of air gap. Therefore, it shows rod-plane of 10 mm gap length has more uniform electric field rather than other gap length while plane-plane electrodes have achieved uniform electric field because the highest E_{max} occurred on the along the top of electrode.

4.5 Comparison between Calculation and Simulation

Further tests have been carried out to obtain E_{max} curves between calculation and simulation for uniform and non-uniform field configuration as Table 4.6 below. The error between these results can be calculated by using formula in equation

$$Error(\%) = \frac{|\ Calculation - Simulation\ |}{|Calculation\ |} \times 100\% \tag{4.5}$$

Table 4.6: The comparison of error between calculation and simulation results.

	Gap length (mm)	Calculation E_{max} (kV/mm)	Simulation E_{max} (kV/mm)	Error (%)
Plane-Plane	**5**	3.04	3.00	1.32
	10	2.07	2.05	0.97
	15	2.06	2.03	1.46
	20	1.82	1.80	1.10
Rod-Plane	**10**	2.88	3.10	7.10
	20	2.32	2.50	7.20
	30	2.09	2.10	0.48
	40	2.06	2.00	2.91
	50	2.05	1.98	3.41

Referring to Table 4.6, the range of error for plane-plane electrode configuration is between 0.97 until 1.46 %. Besides, there are only slightly difference in percentage error which

is from 5 to 20 mm air gap length. For rod-plane electrode configuration, the range of error is between 0.48 until 7.20 % and there are big errors especially for 10 and 20 mm air gap length. There are possibilities the factor of parameters like humidity, temperature and pressure were influenced the big error while run the experiment. The comparison between calculation and simulation for plane-plane field configuration was shown in Figure 4.13 while Figure 4.14 shows the comparison between calculation and simulation for rod-plane field configuration.

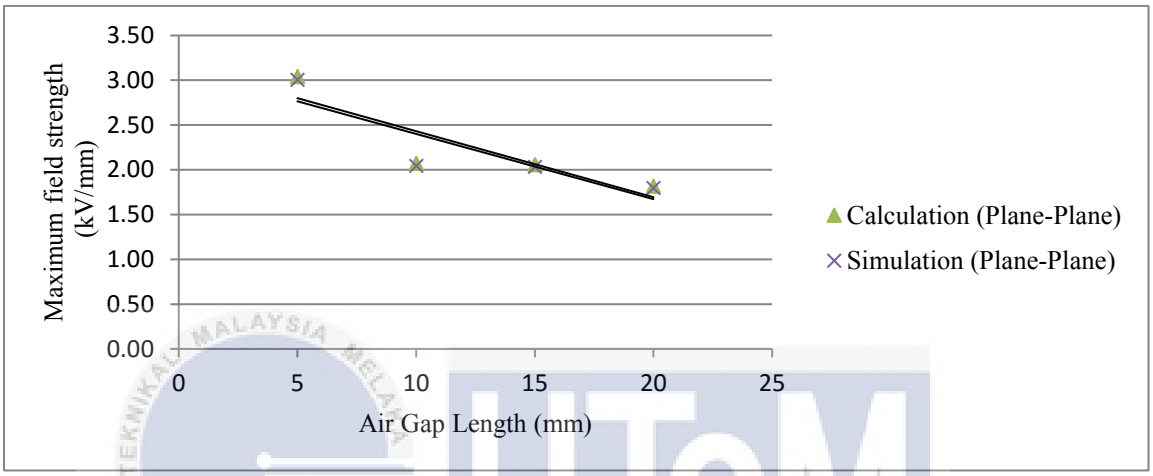

Figure 4.13: The comparison between calculation and simulation for plane-plane field configuration.

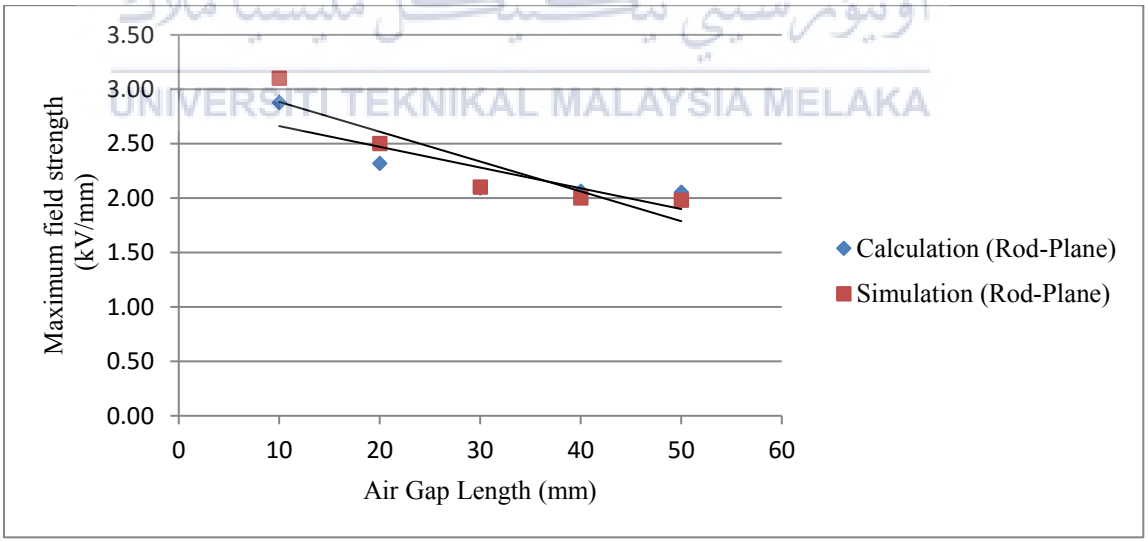

Figure 4.14: The comparison between calculation and simulation for rod-plane field configuration.

As depicted in Figure 4.13 above, the graph of E_{max} for calculation and simulation were approximately to each other while the graph of E_{max} in Figure 4.14 were decreased as gap

length increases. It was clear that the graph of simulation is higher than the graph of calculation. While comparing with the experimental, theoretical and simulation results it is observed that the electric field decreases as the distance between electrodes increases. Both approaches show a very sharp decrease in maximum electric field as the gap length increases. The breakdown voltage of uniform field configurations was higher than non-uniform field configurations. This is valid with the ionization process during conduction and breakdown in gases as when the humidity and temperature increases, the process of ionization by collision, electrons starting at the cathode were accelerated more and more between collisions with other gas molecules when traveling to anode [2]. Furthermore, when there are a lot of energy, ε gained rather than ionization potential, V_i during this travel, then ionization can easily take place.

4.4 Summary

From this study, the finite element method is important in viewing the behaviour of electric fields under various circumstances, such as the effects of gap length between electrodes and the effects of the geometry of the electrodes themselves. In this study, a model for COMSOL Multiphysics modelling has been developed.

Fundamental tests on air breakdown have been carried out to investigate the U_{50} behavior of air in various test conditions. The results are corrected according to the correction factors defined by the standard in BS EN 60060-1 2010 to ensure the accuracy of the results are reliable. The values of U_{50} are then used to determine the E_{max} using COMSOL Multiphysics software. This is used to give a better understanding of the highest stress region inside the test vessel. Besides, electric field can also be plotted along the surface of the high voltage electrodes if desired. It was found that although low values of breakdown voltage in plane-plane and rod-plane occurred, E_{max} can be determined at the highest breakdown level among all the field configurations.

CHAPTER 5

CONCLUSIONS AND RECOMMENDATIONS

5.1 Conclusions

An extensive review of pervious work air breakdown voltage and finite element method (FEM) have been presented. The topics covered include power system applications, air breakdown mechanism, classical gas laws, estimation and control of electric stress and numerical methods for computation of electric field. Air is the most necessary gas used for insulating purposes, it has a unique feature of being universally and immediately available at no cost. Atmospheric air is the cheapest and most widely used dielectric. The electric breakdown strength of an air-insulated gap between different metal electrodes can be enhanced considerably by an experiment

In order to improve the fundamental characteristics of the air breakdown and knowledge of electric field in numerous high voltage applications, a test has been developed specially for air breakdown research work, which include a test vessel, control measures and atmospheric pressure. Other control measures include humidity, temperature and pressure readings. The humidity and temperature are read wirelessly and based on the readings, the necessary atmospheric corrections can be made according to standards.

Average mean value of breakdown voltage, U_{50} were carried out to examine the breakdown performance of air for uniform and non-uniform field configuration. Moreover, atmospheric corrections in dry tests, in accordance BS EN 60060-1 2010 standard, were carried out. As it is important to validate all test results, temperature and humidity controls were place inside the test vessel. There are two different electrode configurations were used in the air breakdown tests, namely the rod-plane and plane-plane electrode configurations which are 12

mm diameter of rod electrode and 100 mm diameter of plane electrode. The effects of electrode geometry and gap lengths between the electrodes were also investigated. The results were determined the electric field based on models for each electrode configuration. With a proper model in the computational works, the location of the maximum electric field was determine for each electrode configuration.

As for uniform field configuration, the values of U_{50} were increased approximately linearly with the pressure of 1 atm and E_{max} values are almost the same for every gap length. As U_{50} was increased, the ability of air to withstand E_{max} (and high stress) was decreased before and after correction. Furthermore, various factors that affect the dielectric strength of air was influenced by atmospheric conditions and humidity. The air density like temperature and pressure can affect the data results of experiments. While for non-uniform field configuration, the values of U_{50} was showed that a bigger gap length in electrode configuration will introduce a slightly bigger increase in U_{50} with the pressure of 1 atm. Furthermore, there are only small differences occur between U_{50} before and after correction while for curve of E_{max} decreased as U_{50} increased.

In order to investigate behaviour under electric field, there are some numerical methods for solving partial different equations which consists of Laplace's and Poisson's equation which are Finite Element Method (FEM), Finite Difference Method (FDM), Charge Simulation Method (CSM) and Boundary Element Method (BEM) were used in computational works. However, in this study, FEM was selected for the calculation of electric fields.

A simulation model was developed based on each test condition, which consists of three stages of pre-processing, solving and post-processing. There are a few parameters need to consider as permittivity of air, free space permittivity and space charge density. Material used, boundary conditions, mesh, execute mode are applied. The computational modelling made use of axis-symmetric features of the test vessel, which consumed less time in computing and although it is in 2D, the results of the simulation were accurate. Only small discrepancies were noted between simulated results and calculated results.

For simulation results, the magnitude of the electric strength is represented by colour shades for uniform and non-uniform field configuration. For plane-plane electrode configurations, E_{max} was present a very high stress region and eventually pre-discharge was began to occur. The air breakdown is started at the top of high voltage electrode until the surface

of the ground electrode. Besides, E_{max} for rod-plane electrode configuration was occurred at the tip of the rod which is right on the central longitudinal axis of the rod. It is most likely location where the pre-discharges will occur and followed by air breakdown. The electric field effects were quantified and the influence of electrode geometry and configuration can be further investigated.

5.2 Recommendations

Based on the work carried out in this study, the following areas have been identified for related future investigations:

a) Investigations on more electrode profiles: As it is important to understand properly the behaviour of air breakdown under various electric fields, other electrode configurations can be adopted in future investigations to represent more field utilization factor. Sphere air gap electrode and Rogowski profile electrodes are suggested for future work.

b) Other gas insulation: The investigation of insulating and quenching media of sulphur hexafluoride (SF_6) can be the alternative way than air insulation. Based on reading and research from previous work, gas insulated substations (GIS) primarily used SF_6 gas as the primary insulator as SF_6 is non-toxic, maintains atomic and molecular properties even at high voltages, high cooling properties and superior arc quenching properties [13].

REFERENCES

[1] P. B. Sankar, "Measurement of Air Breakdown Voltage and Electric Field Using Standard Sphere Gap Method," *Master Thesis*, no. 10, pp. 5–16, 2011.

[2] V. K. M S Naidu, "Conduction and Breakdown in Gases," in *High Voltage Engineering*, Third Edit., Mc Graw Hill, 2004, pp. 27–68.

[3] E. Onal, "Breakdown Characteristics of Gases in Non-Uniform Fields," *J. Electr. Electron. Eng. - Istanbul Univ.*, vol. 4, no. 2, pp. 1177–1182, 2004.

[4] G. R. Jones, M. A. Laughton, and M. G. Say, *Electrical Engineer's Reference Book*, Fifteenth. Butterworth Heinemann Limited.

[5] a Kara, Ö. Kalenderli, and K. Mardikyan, "Effect of Dielectric Barriers To the Electric Field of Rod-Plane Air Gap," *COMSOL Conf. 2006*, 2006.

[6] F. Miron, M. Purcar, and C. Munteanu, "Numerical Computation of the Electromagnetic Field inside a High Voltage Substation," vol. 56, no. 4, pp. 175–178, 2015.

[7] M. S. Kamarudin, "Experimental Investigation of CF_3I-CO_2 Gas Mixtures on the Breakdown Characteristics in Uniform and Non-Uniform Field Configurations," no. June, 2013.

[8] J. H. Cloete and J. Van Der Merwe, "The breakdown electric field between two conducting spheres by the method of images," *IEEE Trans. Educ.*, vol. 41, no. 2, pp. 141–145, 1998.

[9] P. G. Slade and E. D. Taylor, "Electrical Breakdown in Atmospheric Air Between Closely Spaced (0 . 2 m – 40 m) Electrical Contacts," vol. 25, no. 3, pp. 390–396, 2002.

[10] N. Solutions and F. D. Method, "Analytical versus Numerical Solutions," pp. 1–4.

[11] M. Curti, J. J. H. Paulides, and E. A. Lomonova, “An Overview of Analytical Methods for Magnetic Field Computation,” 2015.

[12] “Working of Air Circuit Breakers | StudyElectrical | Online Electrical Engineering Study Site.” [Online]. Available: http://www.studyelectrical.com/2014/12/working-of-air-circuit-breakers.html. [Accessed: 02-Apr-2017].

[13] “Gas insulated VS Air insulated substations.” [Online]. Available: http://engineering.electrical-equipment.org/others/gas-insulated-vs-air-insulated-substations.html. [Accessed: 02-Apr-2017].

[14] J R Lucas, J. R. Lucas, E. Kuffel, W. S. Zaengl, and J. Kuffel, “High Voltage Engineering, Fundamentals,” *High Volt. Eng.*, vol. 1, no. c, p. 552, 2001.

[15] C. L. Wadhwa, “Breakdown Mechanism of Gaseous, Liquid and Solid Materials,” *High Volt. Eng.*, pp. 1–55, 271AD.

[16] E. E. Kunhardt, “Electrical Breakdown of Gases: The Prebreakdown Stage,” *IEEE Trans. Plasma Sci.*, vol. 8, no. 3, pp. 130–138, 1980.

[17] A. Srikant, “Simulation of air breakdown mechanism using different electrodes,” p. 35, 2011.

[18] R. Arora and W. Mosch, *High Voltage Insulation Engineering*, First Edit. New Delhi: New Age International (P) Limited, 2004.

[19] D. J. Holtzhausen and D. W. Vosloo, “High Voltage Engineering Practice and Theory, Draft Version of Book,” p. 157, 2011.

[20] S. Africa and R. Klrkpatiilck, “The Maximum Electric Field Strength For Several Simple Electrode Configurations,” vol. vii, no. 20, pp. 120–126, 1897.

[21] K. L. Kaiser, *Electrostatic Discharge*. New York: Taylor & Francis, 2006.

[22] V. G. Schematic, “Electric Field Distribution,” pp. 2–5, 2016.

[23] H. Javadi and M. Farzaneh, “Electric Field Calculations in Rod-plane Gap Using Hyperbolic Approximation and Finite Element Method : a Comparison,” *Network*, pp. 1–7.

[24] "BS EN 60060-1 : 2010 BSI Standards Publication High-voltage test techniques Part 1 : General definitions and test requirements," 2010.

[25] H. Javadi, M. Farzaneh, and A. Peyda, "Determination of electric field at inception based upon current-voltage characteristics of AC corona in rod-plane gaps," *Iran. J. Electr. Electron. Eng.*, vol. 6, no. 2, pp. 119–128, 2010.

[26] H. Ekram, Nandagopal, and B. . Prabhakar, "Effect of humidity on breakdown voltages of gaps and insulators," 1974.

[27] D. Rodriguez, R. S. Gorur, and P. M. Hansen, "Effect of humidity on the breakdown characteristics of air in non-uniform fields at 30 kHz," *IEEE Trans. Dielectr. Electr. Insul.*, vol. 17, no. 1, pp. 45–52, 2010.

[28] M. Li, F. Sahlen, W. Dong, G. Asplund, and B. Jacobson, "Humidity effects on dielectric strength of air-gaps for indoor HV installations," *Annu. Rep. - Conf. Electr. Insul. Dielectr. Phenomena, CEIDP*, vol. 2005, pp. 43–46, 2005.

[29] M. Valavala and B. Kanchanapalli, "Breakdown mechanism in air insulating medium by an experimental study," vol. 47, pp. 8832–8835, 2012.

LIST OF APPENDICES

Appendix A : Project Gantt Chart

Year	Final Year Project 2				
Task	**2**	**3**	**4**	**5**	**6**
Title selection and PSM briefing					
Literature review of previous related works					
Conduct the experiment					
Collecting data or information from the experiment					
Analysis the result					
Report writing and preparation for presentation					
Report submission					

Appendix B : Key Milestone

Milestone	Project Task	Expected Date
1	Literature Review on the air breakdown mechanism	Dec 2016
2	Conduct the experiment	February 2017
3	Perform air breakdown voltage test and collect all data or information from the experiment. Simulate the simulation by using different electrodes configuration using COMSOL Multiphysics software.	March 2017

4	Analysis the result from the experiment and simulation to make hypothesis in order to fulfil the objective of this study.	April 2017
5	Report writing and preparation for the presentation.	May 2017
6	Report submission and presentation	June 2017

Appendix C : The values of AC air breakdown voltage

Test : Air

Electrode Configuration : Plane-Plane

Gap length	**5mm**	**10mm**	**15mm**	**20mm**
Ambient Temperature (℃)	30	28.9	29.8	29.4
Humidity (%)	82	82	82	82
Test No.	RMS (kV)	RMS (kV)	RMS (kV)	RMS (kV)
1	13.9	17.33	29.3	32.4
2	14	17.8	29.4	32.14
3	14.61	17.4	29.4	32.6
4	14.46	18	29.4	33.5
5	13.74	18.1	29.5	33
6	14.45	18.23	29.5	33.8
7	14.8	18.8	29.4	33.8
8	14.57	19.1	29.5	33.7
9	14.27	19.28	29.5	34.7
10	15.17	19	29.4	33.8
11	14.4	19	29.5	34.8
12	13.92	20.6	29.7	34.9
13	13.69	19.5	29.5	34.7
14	14.13	20.78	29.6	35
15	14.6	19.6	29.7	34.8
16	14.47	18.36	29.5	34.5

17	14.26	19.5	29.51	35
18	14.71	20.07	29.6	35.2
19	14.25	19.6	28.7	35.1
20	14.09	19.47	29.7	35.3
21	14.69	20	29.5	35.1
22	14.69	20.1	29.5	35.1
23	14.5	20.18	29.5	35.2
24	14.75	20.3	29.4	35.1
25	14.77	20.4	29.5	35.3
26	14.59	20.18	29.4	35.3
27	14.69	20.3	29.5	35.3
28	15.4	20.6	29.5	35.2
29	14.5	19.25	29.62	35.1
30	14.52	20.1	29.5	35.2
31	13.95	20.5	29.62	35
32	15	20.4	29.4	35.2
33	14.86	20.61	29.5	35.4
34	14.68	20.36	28.4	35.3
35	15.18	20.6	29.5	35.4
36	14.46	20.6	29.6	35.3
37	14.83	20.5	29.5	35.1
38	15	20.6	29.7	35.4
39	14.6	20.7	29.5	35.4
40	14.49	20.7	29.6	35.4
41	14.16	20.7	29.5	35.4
42	15.03	20.8	29.57	35.5
43	15.2	20.6	29.62	35.6
44	15.08	20.6	29.4	31.94
45	14.71	20.6	29.5	35.3
46	14.07	20.7	29.65	35.4
47	14.48	20.8	29.4	35.6
48	15.3	20.5	29.5	35.5

49	13.7	20.8	29.62	35.5
50	13.75	19.3	29.5	35.6

Test : Air

Electrode Configuration : Rod-Plane

Gap length	**10mm**	**20mm**	**30mm**	**40mm**	**50mm**
Ambient Temperature (℃)	28.2	29.3	29.3	29.2	30.1
Humidity (%)	82	77	77	77	76
Test No.	RMS (kV)	RMS (kV)	RMS (kV)	RMS (kV)	RMS (kV)
1	15.26	17.7	19	22.44	24.22
2	15.87	16.91	21.56	22.5	23.56
3	12.79	17.12	19.28	22.39	23.76
4	15.4	17.45	19.84	22.19	23.33
5	15.71	17.81	20.24	21.73	24.11
6	15.52	18.09	20.67	22.7	24.93
7	15.6	18.6	18.51	21.76	23.76
8	16.21	17.71	19.73	22.17	23.7
9	16.38	18.13	19.11	21.27	24.71
10	16.51	17.83	20.04	21.56	23.56
11	16.34	18.01	20.73	21.44	23.36
12	15.86	17.02	18.79	22.65	23.1
13	15.49	17.07	19.16	22.76	23.36
14	15.81	17.48	19.09	22.76	24.28
15	15.78	18.33	21.1	21.22	22.93
16	16.17	16.31	19.98	22.21	23.73
17	15.52	18	21.47	22.67	22.39

18	15.35	17.34	22.1	22.9	23.56
19	16.46	18.34	20.27	22.3	22.73
20	16.15	17.01	20.16	22.1	23.79
21	16.5	17.98	20.76	22.44	22.48
22	16.06	16.17	20.47	22.87	22.82
23	15.68	18.39	19.73	21.9	23.85
24	16.16	18.34	21.21	21.16	22.51
25	15.94	16.44	20.21	22.59	23.48
26	15.25	18.44	20.21	22.36	22.11
27	15.28	18.84	20.9	22.13	22.65
28	16.32	17.12	20.53	22.96	22.33
29	15.88	18.41	20.13	21.76	22.68
30	15.84	18.37	20.58	22.99	22.05
31	16.05	18.32	21.24	21.59	22.88
32	15.65	18.73	20.1	22.59	22.93
33	16.45	18.62	20.76	22.99	23.45
34	15.75	18.32	20.73	22.13	22.31
35	15.46	17.64	21.36	22.36	22.02
36	16.31	17.89	19.7	23.88	22.05
37	15.42	17.63	20.56	22.39	23.78
38	15.37	17.48	21.53	22.36	23.51
39	15.39	19.9	21.56	21.19	23.82
40	15.38	17.55	20.53	22.22	21.68
41	15.84	18.72	21.07	23.42	22.42
42	15.87	18.2	21.56	22.36	22.05

43	15.41	18.99	20.96	22.64	23.22
44	15.66	18.88	19.07	21.93	23.56
45	15.98	17.33	21.87	22.16	23.85
46	15.5	18.29	19.34	22.1	22.73
47	15.79	17.26	20.84	22.5	24.65
48	15.54	18.19	19.38	22.22	22.71
49	15.45	17.48	20.96	23.19	22.31
50	15.11	18.44	22.04	22.19	21.19

Appendix D : Model Parameters

Parameter	Symbol	Value
Permittivity of free space	ε_0	$8.854x10^{-12}$ F.m^{-1}
Relative permittivity of air	ε_r	1
Space charge density	ρ	0

Appendix E : BS EN 60060-1 2010 (high-voltage test techniques)

BS EN 60060-1:2010

BSI Standards Publication

High-voltage test techniques

Part 1: General definitions and test requirements

4.3 Atmospheric corrections in dry tests

4.3.1 Standard reference atmosphere

The standard reference atmosphere is:

- temperature t_0 = 20 °C ;
- absolute pressure p_0 = 1 013 hPa (1 013 mbar) ;
- absolute humidity h_0 = 11 g/m^3.

NOTE 1 An absolute pressure of 1 013 hPa corresponds to the height of 760 mm of the mercury column in a mercury barometer at 0 °C. If the barometer height is H mm of mercury, the atmospheric pressure in hectopascal is approximately:

$$p = 1{,}333\ H \text{ hPa}$$

Correction for temperature with respect to the height of the mercury column is considered to be negligible.

NOTE 2 Instruments automatically correcting pressure to sea level are not suitable and should not be used.

4.3.2 Atmospheric correction factors for air gaps

The disruptive discharge of external insulation depends upon the atmospheric conditions. Usually, the disruptive-discharge voltage for a given path in air is increased by an increase in either air density or humidity. However, when the relative humidity exceeds about 80 %, the disruptive-discharge voltage becomes irregular, especially when the disruptive discharge occurs over an insulating surface.

Appendix F : Manual Calculation Correction Factor of Plane-Plane for 10 mm

t_0 = 20℃

p_0 = 1013 hPa (1013 mbar)

Step 1 : Calculate δ	$\delta = \frac{p}{p_0} \times \frac{273 + t_0}{273 + t}$ $= \frac{1000}{1013} \times \frac{273 + 20}{273 + 28.9}$ $= 0.9581$
Step 2 : Calculate h	$h = \frac{6.11 \times R \times e^{\frac{17.6 \times t}{243+t}}}{0.4615 \times (273 + t)}$ $= \frac{6.11 \times 82 \times e^{\frac{17.6 \times 28.9}{243+28.9}}}{0.4615 \times (273 + 28.9)}$ $= 23.3480$
Step 3 : Calculate k	$(AC, k = 1 + 0.012(\frac{h}{\delta} - 11)$ $= 1 + 0.012(\frac{23.3480}{0.9581} - 11)$ $= 1.1604$
Step 4 : Calculate g	$g = \frac{U_{50}}{500 \times L \times \delta \times k}$ $= \frac{19.84}{500 \times 0.01 \times 0.9581 \times 1.1604}$ $= 3.5691$
Step 5 : Calculate m and w Based on Table 3.2, when g is 5.1581 which is g > 2.0, m is 1.0 and w is 0.	
Step 6 : Calculate k_1	$k_1 = \delta^m$ $= 0.9581^{1.0}$ $= 0.9581$
Step 7 : Calculate k_2	$k_2 = k^w$ $= 1.1604^0$ $= 1.000$
Step 8 : Calculate K_t	$K_t = k_1 k_2$

	$= (0.9581)(1.0000)$ $= 0.9581$
Step 9 : U_0	$U_0 = {}^{U}/_{K_t}$ $= {}^{19.84}/_{0.9581}$ $= 20.71kV$

Appendix G : Manual Calculation Correction Factor of Rod-Plane for 10 mm

t_0 = 20℃

p_0 = 1013 hPa (1013 mbar)

Step 1 : Calculate δ	$\delta = \frac{p}{p_0} \times \frac{273 + t_0}{273 + t}$ $= \frac{1000}{1013} \times \frac{273 + 20}{273 + 28.2}$ $= 0.9603$
Step 2 : Calculate ${}^{h}/_{\delta}$	$h = \frac{6.11 \times R \times e^{\frac{17.6 \times t}{243+t}}}{0.4615 \times (273 + t)}$ $= \frac{6.11 \times 82 \times e^{\frac{17.6 \times 28.2}{243+28.2}}}{0.4615 \times (273 + 28.2)}$ $= 22.4712$
Step 3 : Calculate k	$AC, k = 1 + 0.012 \left(\frac{h}{\delta} - 11\right)$ $= 1 + 0.012 \left(\frac{22.4712}{0..9603} - 11\right)$ $= 1.1488$
Step 4 : Calculate g	$g = \frac{U_{50}}{500 \times L \times \delta \times k}$ $= \frac{15.7294}{500 \times 0.01 \times 0.9603 \times 1.1488}$ $= 2.8516$
Step 5 : Calculate m and w	

Based on Table 3.2, when *g* is 2.8516 which is g > 2.0, *m* is 1.0 and *w* is 0.	
Step 6 : Calculate k_1	$k_1 = \delta^m$ $= 0.9603^{1.0}$ $= 0.9603$
Step 7 : Calculate k_2	$k_2 = k^w$ $= 1.1488^0$ $= 1.0000$
Step 8 : Calculate K_t	$K_t = k_1 k_2$ $= (0.9603)(1.0000)$ $= 0.9603$
Step 9 : U_0	$U_0 = {}^{U}/_{K_t}$ $= {}^{15.7294}/_{0.9603}$ $= 16.3798\ kV$

Appendix H: Correction Factor

i) Plane-Plane Electrode Configuration

Gap length (mm)	5	10	15	20
Atmospheric conditions				
Temperature, (℃)	30	28.9	29.8	29.4
Humidity, RH (%)	82	82	82	82
h	24.79	23.35	24.52	23.99
Air density correction				
$\boldsymbol{\delta}$	0.9546	0.9581	0.9552	0.9565
m	1	1	1	1
$\boldsymbol{k_1 = \delta^m}$	0.9546	0.9581	0.9552	0.9565
Humidity correction				
k	1.1796	1.1604	1.1760	1.1690
w	0	0	0	0
$\boldsymbol{k_2 = k^w}$	1	1	1	1
$\boldsymbol{K_t}$	0.9546	0.9581	0.9552	0.9565
Application of correction factors				
$\boldsymbol{U_{50}}$ **(kV)**	15.21	20.71	30.86	36.36

ii) Rod-Plane Electrode Configuration

Gap length (mm)	10	20	30	40	50
Atmospheric conditions					
Temperature, (℃)	28.2	29.3	29.3	29.2	30.1
Humidity, RH (%)	82	77	77	77	76
h	22.47	22.41	22.41	22.29	23.10
Air density correction					
$\boldsymbol{\delta}$	0.9603	0.9568	0.9568	0.9571	0.9543
m	1	1	1	1	0.6643
$\boldsymbol{k_1 = \delta^m}$	0.9603	0.9568	0.9568	0.9571	0.9694
Humidity correction					
k	1.1488	1.1490	1.1490	1.1474	1.1584
w	0	0.2666	0.9165	1.0000	0.6643
$\boldsymbol{k_2 = k^w}$	1	1.0377	1.1358	1.1474	1.1026
$\boldsymbol{K_t}$	0.9603	0.9929	1.0867	1.0982	1.0689
Application of correction factors					
$\boldsymbol{U_{50}}$ **(kV)**	16.38	18.02	18.79	20.31	21.61